


## Roughness and critical force for depinning at 3-loop order

 Mikhail N. Semeikin and Kay Jörg Wiese<sup>\*</sup>

 CNRS-Laboratoire de Physique de l'École Normale Supérieure, PSL, ENS, Sorbonne Université,  
 Université Paris Cité, 24 rue Lhomond, 75005 Paris, France

 (Received 15 January 2024; revised 22 March 2024; accepted 22 March 2024; published 18 April 2024)

A  $d$ -dimensional elastic manifold at depinning is described by a renormalized field theory, based on the functional renormalization group (FRG). Here, we analyze this theory to 3-loop order, equivalent to third order in  $\epsilon = 4 - d$ , where  $d$  is the internal dimension. The critical exponent reads  $\zeta = \frac{\epsilon}{3} + 0.04777\epsilon^2 - 0.068354\epsilon^3 + O(\epsilon^4)$ . Using that  $\zeta(d=0) = 2^-$ , we estimate  $\zeta(d=1) = 1.266(20)$ ,  $\zeta(d=2) = 0.752(1)$ , and  $\zeta(d=3) = 0.357(1)$ . For Gaussian disorder, the pinning force per site is estimated as  $f_c = \mathcal{B}m^2\rho_m + f_c^0$ , where  $m^2$  is the strength of the confining potential,  $\mathcal{B}$  a universal amplitude,  $\rho_m$  the correlation length of the disorder, and  $f_c^0$  a nonuniversal lattice-dependent term. For charge-density waves, we find a mapping to the standard  $\phi^4$  theory with  $O(n)$  symmetry in the limit of  $n \rightarrow -2$ . This gives  $f_c = \tilde{A}(d)m^2 \ln(m) + f_c^0$ , with  $\tilde{A}(d) = -\partial_n[\nu(d, n)^{-1} + \eta(d, n)]_{n=-2}$ , reminiscent of logarithmic conformal field theories.

 DOI: [10.1103/PhysRevB.109.134203](https://doi.org/10.1103/PhysRevB.109.134203)

### I. INTRODUCTION

Many disordered elastic systems undergo a depinning transition. Examples are magnetic domain walls [1–8], earthquakes [9–16], contact lines [17–24], vortex lattices [25–29], charge-density waves (CDWs) [14,25,30–32], and many more, see the recent review [33].

They all evolve via an overdamped Langevin equation for the position  $u(x, t)$  of site  $x$  at time  $t$ :

$$\eta\partial_t u(x, t) = \nabla^2 u(x, t) + m^2[w - u(x, t)] + F(x, u(x, t)). \quad (1)$$

The second term on the right-hand side stems from a confining potential of strength  $m^2$ , centered at  $w$ . Increasing  $w$  adiabatically slowly drives the system. The last term  $F(x, u)$  is a short-range correlated random force, possibly the  $u$  derivative of a random potential. It is assumed to be Gaussian with variance (connected part):

$$\overline{F(x, u)F(x', u')^c} = \delta^d(x - x')\Delta_0(u - u'). \quad (2)$$

The overbar denotes a disorder average.

The field theory of depinning is by now well established (see the review [33]). It relies on a functional renormalization group (FRG) for the disorder correlator  $\Delta(u)$ , starting from the microscopic disorder  $\Delta_0(u)$ . This idea, already present in the seminal works of Wilson [34] and Wegner and Houghton [35], was recognized as crucial by Fisher [36–38], Middleton and Fisher [39], Narayan and Fisher [40–42], and Balents and Fisher [43] as well as Nattermann *et al.* [44] and Leschhorn *et al.* [45]. Later, Chauve *et al.* [46] and Le Doussal *et al.* [47,48] showed that, both in equilibrium and at depinning, a consistent field theory exists up to 2-loop order. This field theory allows us to deal with the many nontrivial observables arising for pinned manifolds and especially to treat quantitatively avalanches [49–59], including their distributions of

size, velocity, and shape in good agreement with simulations [50,51,60] and experiments [6].

Systems at depinning are characterized by a jerky motion for their centers of mass  $u_w$ :

$$u_w := \frac{1}{L^d} \int d^d x u(x, t). \quad (3)$$

Here,  $L$  is the size of the system, and the integral is evaluated once all motion has stopped. The index  $w$  refers to the position of the confining potential, which is adiabatically slowly moved forward. The central ingredient of the field theory is the renormalized force correlator, defined by the connected average:

$$\Delta(w - w') := m^4 L^d \overline{(w - u_w)(w' - u_{w'})^c}. \quad (4)$$

On one hand, it can be calculated in a loop expansion, equivalent to an expansion in  $\epsilon = 4 - d$ , where  $d$  is the internal dimension of the manifold. On the other hand, the prescription in Eq. (4) can be tested in simulations [61,62] and experiments [8,63–65]. For equilibrium, the loop expansion was extended to 3-loop order in Refs. [66,67]. Here, we report 3-loop results for the  $\beta$  function and the critical force at depinning. Our first central result is the roughness exponent  $\zeta$ :

$$\zeta = \frac{\epsilon}{3} + 0.0477709715\epsilon^2 - 0.0683544(2)\epsilon^3 + O(\epsilon^4). \quad (5)$$

It can numerically be measured by considering the finite-size scaling of the 2-point function in the limit of  $m \rightarrow 0$ :

$$\int_{x,y} \overline{[u(x) - u(y)]^2} \sim L^{2d+2\zeta}, \quad (6)$$

or for a finite  $m$ :

$$\overline{[u(x) - u(y)]^2} \sim m^{-2\zeta} \quad \text{for } m|x - y| \gg 1. \quad (7)$$

The second relevant observable is the critical force per site (force density):

$$f_c := m^2 \overline{(w - u_w)} \equiv -\overline{F(x, u(x, t))}. \quad (8)$$

<sup>\*</sup>wiese@lpt.ens.fr

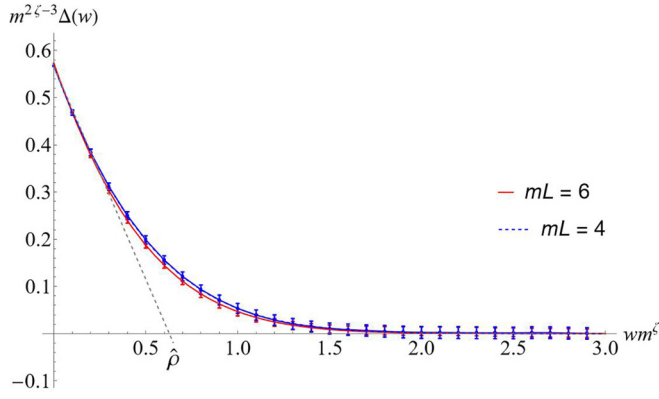


FIG. 1.  $\tilde{\Delta}(w)$  for  $mL = 4$  (blue, top curve) and  $mL = 6$  (red).

The last equality is verified by integrating the equation of motion in Eq. (1), assuming periodic boundary conditions. We show below that

$$f_c = m^2 \overline{(w - u_w)} = f_c^0 - \mathcal{B} m^2 \rho_m, \quad (9)$$

$$\mathcal{B} = 1 - 0.30998\epsilon + 0.570136\epsilon^2 + O(\epsilon^3). \quad (10)$$

Here,  $f_c^0$  has a lattice-dependent (but  $m$ -independent) value,  $\mathcal{B}$  is a universal amplitude,  $m^2$  is given by the experiment, and  $\rho_m$  is a length scale in the driving direction set by the disorder, see Fig. 2:

$$\rho_m := \frac{\Delta(0)}{|\Delta'(0^+)|} \simeq \tilde{\rho} m^{-\zeta}. \quad (11)$$

An example for  $\Delta(w)$  is given in Fig. 1. For small  $m$ ,  $f_c$  converges to  $m^{2-\zeta}$  times a system-specific amplitude  $\tilde{\rho}$ , set by the microscopic disorder. While  $\rho_m$  needs to be measured, the confining potential strength  $m^2$  is imposed in the simulation or experiment. Should it be unknown or insufficiently well known in the experiment [68], it can be extracted from the linear part of the force-extension curve.

The amplitude  $\mathcal{B}$  in Eq. (10) is universal, independent of microscopic details. This is a quite astonishing result, as it is rarely possible to have a universal amplitude rather than a universal exponent. As we will see below, the reason this happens here is that the diagrammatic result does not resum into a power law in  $m$ , but instead, it depends logarithmically on

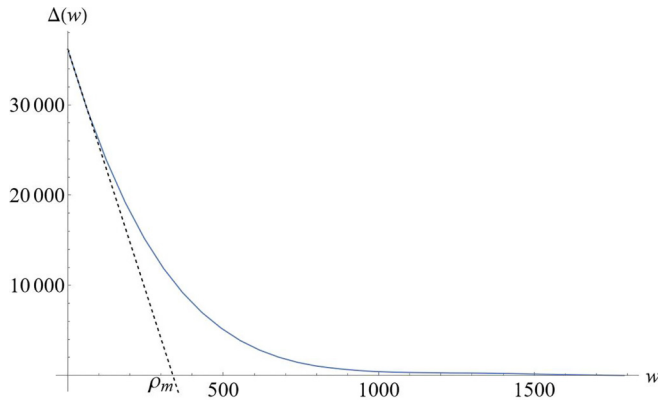


FIG. 2.  $\Delta(w)$  for  $mL = 6$  (blue) and  $L = 1024$ . The tangent at  $w = 0$  defines the correlation length  $\rho_m$ .

$m$ , and varying  $\mathcal{B} \ln m$  gives back  $\mathcal{B}$ . The final result contains a power law since it is still multiplied by  $\rho_m$ . We explain this in detail in Sec. IV.

The situation is even more extraordinary for CDWs, for which  $\zeta = 0$ . As we discuss in Sec. V, CDWs can be mapped onto the  $O(n)$  model in the limit of  $n \rightarrow -2$ . For this case, Eqs. (9) and (10) reduce to

$$\frac{f_c}{m^2} = \text{const.} - \tilde{\mathcal{A}}(d) \ln(m), \quad (12)$$

$$\tilde{\mathcal{A}}(d) = -\partial_n [v(d, n)^{-1} + \eta(d, n)]_{n=-2}. \quad (13)$$

Here,  $v(d, n)$  and  $\eta(d, n)$  are the critical exponents  $\nu$  and  $\eta$  of the  $O(n)$  model in dimension  $d = 4 - \epsilon$ . Equations (12) and (13) are reminiscent of logarithmic conformal field theories (log-CFTs) [69,70]: When two operators collide as a function of an external control parameter, here,  $n$ , the renormalization group (RG) flow becomes nondiagonalizable and replaced by a rank-2 Jordan-block form, leading to a universal amplitude in front of a logarithm, very much as in Eqs. (12) and (13).

The remainder of this paper is organized as follows: In Sec. II, we start with the RG analysis for depinning. After a brief reminder of how to perform a FRG and the problems involved, we derive and analyze in Sec. III the RG  $\beta$  function, the critical exponent  $\zeta$ , and the shape of the renormalized disorder correlator. The critical force is treated in Sec. IV. We then specialize to CDWs in Sec. V, which allows us to use high-order RG calculations for the  $O(n)$  model. Section VI confirms our analytical calculations with numerical simulations. Conclusions are offered in Sec. VII. Technical details and results for specific cases are given in various appendices.

## II. RG ANALYSIS

### A. Field theory of the depinning transition, response function

Here, we briefly review the basics of perturbation theory and renormalization for depinning as written in Eq. (1). For a detailed introduction, we refer the reader to section 3 of Ref. [33]. The idea is to discretize the equation of motion in Eq. (1) as

$$u(x, t + \delta t) = u(x, t) + \frac{\delta t}{\eta} [\nabla^2 u(x, t) + m^2 [w - u(x, t)] + F(x, u(x, t))]. \quad (14)$$

For  $x$  and  $t$  fixed, this is achieved by writing, for the expectation  $\langle O \rangle$  of any observable  $O$  depending on  $u(x, t + \delta t)$  [71–76]:

$$\begin{aligned} & \langle O(u(x, t + \delta t)) \rangle \\ &= \frac{\eta}{\delta t} \int_{-\infty}^{\infty} \frac{d\tilde{u}(x, t)}{2\pi i} \int_{-\infty}^{\infty} du(x, t + \delta t) O(u(x, t + \delta t)) \\ & \quad \times \exp \left( \tilde{u}(x, t) \left( \frac{\eta}{\delta t} [u(x, t + \delta t) - u(x, t)] + \nabla^2 u(x, t) \right. \right. \\ & \quad \left. \left. + m^2 [w - u(x, t)] + F(x, u(x, t)) \right) \right). \end{aligned} \quad (15)$$

The integral over  $\tilde{u}(x, t)$  enforces Eq. (14), as in  $\int_{-\infty}^{\infty} \frac{dk}{2\pi} e^{ikx} = \delta(x)$ ; the final integral over  $u(x, t + \delta t)$  ensures that the latter takes its appropriate value, proving Eq. (15).

Note that we have used the so-called Itô discretization, where the right-hand side of Eq. (14) is evaluated at time  $t$ . If one were to take  $t + \delta t/2$  or  $t + \delta t$ , a nontrivial factor would appear.

The strategy forward is now clear: Define the path-integral measure:

$$\int \mathcal{D}[\tilde{u}] \mathcal{D}[u] := \prod_x \prod_t \frac{\eta}{\delta t} \int_{-i\infty}^{i\infty} \frac{d\tilde{u}(x, t)}{2\pi i} \int_{-\infty}^{\infty} du(x, t + \delta t), \quad (16)$$

and action:

$$\begin{aligned} \mathcal{S}[u, \tilde{u}, F] = & \int_{x,t} \tilde{u}(x, t) [(\eta \partial_t - \nabla^2 + m^2)(u(x, t) - w) \\ & - F(x, u(x, t)) - \eta(x, t)]. \end{aligned} \quad (17)$$

The proper definition of  $\eta \partial_t$  is as given in Eq. (15). While  $\tilde{u}(x, t)$  in the path integral is purely imaginary, it can be continued analytically if the integration path remains convergent.

The expectation of an observable  $O$  (which can now depend on any of the variables in the measure) reads

$$\langle O \rangle = \int \mathcal{D}[\tilde{u}] \mathcal{D}[u] \exp(-\mathcal{S}[u, \tilde{u}, F]) O. \quad (18)$$

The final step is to average over disorder, which by assumption is Gaussian with variance given in Eq. (2). Denoting this by an overline, we obtain the disorder-averaged action  $\exp(-\mathcal{S}[u, \tilde{u}]) := \overline{\exp(-\mathcal{S}[u, \tilde{u}, F])}$ , with

$$\begin{aligned} \mathcal{S}[u, \tilde{u}] &= \int_{x,t} \tilde{u}(x, t) [(\eta \partial_t - \nabla^2 + m^2)[u(x, t) - w] - \eta(x, t)] \\ & - \frac{1}{2} \int_{x,t,t'} \tilde{u}(x, t) \Delta_0(u(x, t) - u(x, t')) \tilde{u}(x, t'). \end{aligned} \quad (19)$$

For simplicity of notations, we put  $\eta \rightarrow 1$  in the remainder of this paper. The response function is defined as the answer of the system to a perturbation by the force  $f(x, t)$ , which we add to the right-hand side of Eq. (1):

$$R(x', t' | x, t) := \frac{\delta}{\delta f(x, t)} \overline{u(x', t')} = \langle u(x', t') \tilde{u}(x, t) \rangle. \quad (20)$$

While the overbar indicates a disorder average, the angular brackets denote averages with respect to the action in Eq. (17). In a translationally invariant system,  $R(x', t' | x, t)$  only depends on  $x' - x$  and  $t' - t$  and is denoted by

$$R(x' - x, t' - t) := R(x', t' | x, t). \quad (21)$$

The most convenient representation is the spatial Fourier transform. For the free theory, it reads

$$\begin{aligned} R(k, t) &= \langle u(k, t + t') \tilde{u}(-k, t') \rangle \\ &= \exp(-(k^2 + m^2)t) \Theta(t). \end{aligned} \quad (22)$$

This form allows us to integrate over time, even in the presence of a nontrivial time behavior, as we will see arising in the next section.

## B. Complications due to the nonanalyticity of the disorder

To perform the calculations, we define a graphical notation for the disorder vertex:

$$\begin{array}{c} \bullet \xrightarrow{t'} \\ | \\ \bullet \xrightarrow{t} \end{array} = \Delta(u(x, t) - u(x, t')) \tilde{u}(x, t) \tilde{u}(x, t'). \quad (23)$$

The arrows represent the response fields  $\tilde{u}(x, t) \tilde{u}(x, t')$ ; the dashed line the disorder  $\Delta(u(x, t) - u(x, t'))$ ; and integration over  $x, t$ , and  $t'$  is implicit. (The spatial coordinate  $x$  is not written.)

Let us illustrate the problem with one of the many 2-loop diagrams:



An arrow between two points represents the response function in Eq. (22), with the momentum it carries indicated and time advancing in the direction of the arrow. An arrow entering into a vertex corresponds to a Wick contraction and yields a derivative. Labeling the space coordinates at the bottom left by  $x$ , bottom right by  $y$ , and top by  $z$ , the diagram reads (up to a global prefactor):

$$\begin{aligned} & \int_{k,p} \int_{t_1} \int_{t_2} \int_{t_3} \int_{t_4} \Delta'(u(x, t_2) - u(x, t_1)) \\ & \times \Delta'(u(y, t_4) - u(y, t_3)) \Delta''(u(z, t_5) - u(z, t_6)) \\ & \times R(k, t_3 - t_1) R(k + p, t_2 - t_3) \\ & \times R(p, t_5 - t_2) R(p, t_5 - t_4). \end{aligned} \quad (25)$$

Since the response functions decay exponentially fast, they imply that  $t_1 \approx t_2 \approx t_3 \approx t_4 \approx t_5$ , whereas  $t_6$  and thus  $u(z, t_5) - u(z, t_6)$  are arbitrary time and arbitrary position differences, respectively. Denoting this possibly large difference in position by  $w$ ,  $\Delta''(u(z, t_5) - u(z, t_6)) \rightarrow \Delta''(w)$  can take any (allowed) value. This is not the case for the other arguments, e.g.,

$$\begin{aligned} \Delta'(u(x, t_2) - u(x, t_1)) &\rightarrow \Delta'(u) \quad \text{for } u > 0 \text{ small} \\ &\simeq \Delta'(0^+), \end{aligned} \quad (26)$$

since  $t_2 > t_1$  due to the causality of the response functions  $R$ , and  $u(x, t)$  increases monotonically with time (Middleton theorem [77], see sec. 3.3 of Ref. [33]). The delicate factor is

$$\Delta'(u(y, t_4) - u(y, t_3)) \simeq \Delta'(0^+) \text{sign}(t_4 - t_3), \quad (27)$$

where we have again expanded for small times. It can have both signs. The integral to be performed is proportional to

$$\begin{aligned} & \int_{k,p} \int_{-\infty}^{t_5} dt_2 \int_{-\infty}^{t_2} dt_3 \int_{-\infty}^{t_3} dt_1 \int_{-\infty}^{t_5} dt_4 \exp(-[m^2 + k^2](t_3 - t_1)) \\ & \times \exp(-[m^2 + (k+p)^2](t_2 - t_3)) \\ & \times \exp(-[m^2 + p^2](t_5 - t_2)) \\ & \times \exp(-[m^2 + p^2](t_5 - t_4)) \text{sign}(t_4 - t_3). \end{aligned} \quad (28)$$

Without a sign function, all integrals can be evaluated via a single rule:

$$\int_{-\infty}^t dt' \exp(-[m^2 + k^2](t - t')) = \frac{1}{m^2 + k^2}. \quad (29)$$

In contrast, Eq. (28) leads to the unusual combination:

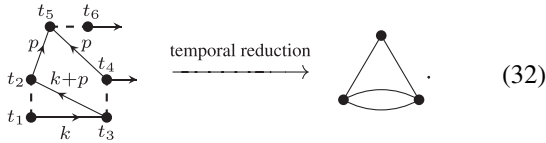
$$\int_{k,p} \frac{1}{[k^2 + m^2][(k+p)^2 + m^2]^2[p^2 + m^2]} - \int_{k,p} \frac{1}{[k^2 + m^2][(k+p)^2 + m^2]^2[(k+p)^2 + p^2 + 2m^2]}. \quad (30)$$

The first line is a standard diagram:

$$\text{triangle} = \int_{k,p} \frac{1}{[k^2 + m^2][(k+p)^2 + m^2]^2[p^2 + m^2]}. \quad (31)$$

In contrast, the second line of Eq. (30) is a genuinely new contribution. What we will see in the following is that, up to 3-loop order, for the effective disorder correlator and the force at depinning, all these new diagrams cancel. In contrast, in dynamic diagrams, i.e., those correcting the dynamic exponent  $z$ , these contributions appear.

In the next section, we list all diagrams contributing to the renormalization of  $\Delta(w)$  up to 3-loop order. Each dynamic diagram, as plotted in Eq. (24), reduces to a static (momentum) diagram upon dropping the temporal information, i.e., dropping the direction in which an arrow goes as well as the times at the vertex. Graphically this amounts to the *temporal reduction*:



$$\text{dynamic diagram} \xrightarrow{\text{temporal reduction}} \text{static diagram}. \quad (32)$$

To alleviate the notations, we only draw the *temporally reduced* (static) representation for each diagram in the next section. This should not be confounded with the momentum integral itself. Surprisingly, for each correction to the disorder, the only momentum integral which survives after summation over all temporal configurations is the *temporally reduced diagram read as a momentum integral*, as in Eq. (31).

### C. Diagrams correcting the disorder

Denoting by  $\delta^{(\ell)}$  the contributions at  $\ell$ -loop order, the corrections to the disorder up to 3-loop order shown in Fig. 3 are given by

$$\delta^{(1)}\Delta(w) = (a), \quad (33)$$

$$\delta^{(2)}\Delta(w) = (A) + (B), \quad (34)$$

$$\delta^{(3)}\Delta(w) = (h) + (i) + (j) + (k) + (l) + (m) + (n) + (o) + (p) + (q). \quad (35)$$

The different diagrams are given in Fig. 4. To simplify the expressions and for easier comparison with the statics, we write the diagrams as minus a total second derivative, such

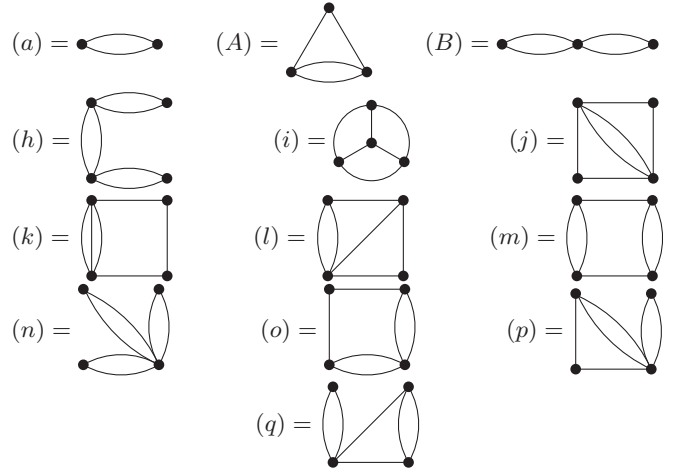


FIG. 3. Diagrams at 3-loop order (without insertion of lower-order counterterms).

that the expression would be the correction to the potential correlator  $R(w)$  [i.e.,  $\Delta(w) = -R'(w)$ ]. The additional terms at depinning, as compared with the statics, are underlined. We note that not all terms can be integrated explicitly, the notable exception being  $\sim \Delta''(w)^2$ .

## III. THE $\beta$ FUNCTION AND ITS FIXED POINT

### A. The $\beta$ function

Using the above diagrams and the integrals tabulated in Appendix A, we write the dimensionfull effective disorder correlator  $\Delta_{\text{eff}}(w)$ :

$$\Delta_{\text{eff}}(w) = \Delta_0(w) + \delta^{(1)}\Delta(w) + \delta^{(2)}\Delta(w) + \delta^{(3)}\Delta(w) + \dots \quad (36)$$

The right-hand side is a function of the bare disorder  $\Delta_0(w)$ , its derivatives, and  $m$ . The  $\beta$  function for the renormalized (effective) dimensionfull disorder correlator  $\Delta_{\text{eff}}(w)$  as a function of the bare disorder  $\Delta_0(w)$  is defined as

$$\begin{aligned} \partial_\ell \Delta_{\text{eff}}(w) &:= -m \partial_m \Delta_{\text{eff}}(w)|_{\Delta_0} \\ &= \epsilon [\delta^{(1)}\Delta(w) + 2\delta^{(2)}\Delta(w) + 3\delta^{(3)}\Delta(w) + \dots]. \end{aligned} \quad (37)$$

There are two steps left: first, rewrite Eq. (36) as a rule:

$$\Delta_0(w) \rightarrow \Delta_{\text{eff}}(w) - \delta^{(1)}\Delta(w) - \delta^{(2)}\Delta(w) - \delta^{(3)}\Delta(w), \quad (38)$$

where, as above,  $\delta^{(i)}\Delta(w)$  are functions of the bare disorder  $\Delta_0(w)$  (and its derivatives). Applying this rule three times to  $\partial_\ell \Delta_{\text{eff}}(w)$  gives  $\partial_\ell \Delta_{\text{eff}}(w)$  as a function of  $\Delta_{\text{eff}}(w)$  instead of  $\Delta_0(w)$ .

In a second step, define

$$\tilde{\Delta}(w) := \epsilon I_1 m^{2\zeta} \Delta_{\text{eff}}(w m^{-\zeta}). \quad (39)$$

This rescaling with  $\epsilon I_1$  and the roughness exponent  $\zeta$  allows us to obtain a fixed point. Rescaling with  $\epsilon I_1 \sim m^{-\epsilon}$  instead of  $m^{-\epsilon}$  eliminates cumbersome numerical factors.

$$\begin{aligned}
& \text{Diagram (a)} : -\iint_w (a) = \frac{1}{2} [\Delta(0) - \Delta(w)]^2 I_1 \\
& \text{Diagram (A)} : -\iint_w (A) = [\Delta'(0^+)^2 \Delta(w) + (\Delta(0) - \Delta(w)) \Delta'(w)^2 - 2\Delta'(0^+)^2 \Delta(w)] I_A \\
& \text{Diagram (B)} : -\iint_w (B) = [\Delta'(0^+)^2 \Delta(w) - \frac{1}{2} (\Delta(0) - \Delta(w))^2 \Delta''(w)] I_B \\
& \text{Diagram (h)} : -\iint_w (h) = [\frac{1}{2} (\Delta(w) - \Delta(0))^2 \Delta''(w)^2 - \Delta'(0^+)^2 \iint_w \Delta''(w)^2] I_h \\
& \text{Diagram (i)} : -\iint_w (i) = [\frac{1}{2} \Delta'(w)^4 - \Delta'(0^+)^2 \Delta'(w)^2 + 4\Delta'(0^+)^2 \Delta''(0) \Delta(w)] I_i \\
& \text{Diagram (j)} : -\iint_w (j) = [(\Delta(w) - \Delta(0))^2 \Delta''(w)^2 - 2\Delta'(0^+)^2 \iint_w \Delta''(w)^2] I_j \\
& \text{Diagram (k)} : -\iint_w (k) = 0 \\
& \text{Diagram (l)} : -\iint_w (l) = 4[\Delta'(w)^2 (\Delta(w) - \Delta(0)) \Delta''(w) - \Delta'(0^+)^2 \Delta''(0) \Delta(w) \\
& \quad + \Delta'(0^+)^2 \Delta''(0) \Delta(w) + \Delta'(w)^2 \Delta'(0^+)^2 - \Delta'(0^+)^2 \iint_w \Delta''(w)^2] I_l \\
& \text{Diagram (m)} : -\iint_w (m) = [\frac{1}{2} \Delta'(w)^4 - \Delta'(0^+)^2 \Delta'(w)^2 + 6\Delta'(0^+)^2 \Delta''(0) \Delta(w) - \Delta'(0^+)^2 \iint_w \Delta''(w)^2] I_m \\
& \text{Diagram (n)} : -\iint_w (n) = [\frac{1}{6} \Delta^{(4)}(w) (\Delta(w) - \Delta(0))^3 \\
& \quad + \Delta'(0^+)^2 ((\Delta(0) - \Delta(w)) \Delta''(w) + \Delta'(w)^2) - \Delta'(0^+)^2 \iint_w \Delta''(w)^2] I_n \\
& \text{Diagram (o)} : -\iint_w (o) = [\Delta'(w)^2 (\Delta(w) - \Delta(0)) \Delta''(w) - \Delta'(0^+)^2 \Delta''(0) \Delta(w) \\
& \quad + \Delta'(0^+)^2 \Delta''(0) \Delta(w) + \Delta'(w)^2 \Delta'(0^+)^2 - \Delta'(0^+)^2 \iint_w \Delta''(w)^2] I_o \\
& \text{Diagram (p)} : -\iint_w (p) = 2[(\Delta(w) - \Delta(0))^2 \Delta^{(3)}(w) \Delta'(w) \\
& \quad + \Delta'(0^+)^2 (\Delta(w) - \Delta(0)) \Delta''(w) - 2\Delta'(0^+)^2 \Delta'(w)^2 + 3\Delta'(0^+)^2 \iint_w \Delta''(w)^2] I_p \\
& \text{Diagram (q)} : -\iint_w (q) = [(\Delta(w) - \Delta(0)) \Delta''(w) (\Delta'(w)^2 - \Delta'(0^+)^2) - 6\Delta'(0^+)^2 \Delta''(0) \Delta(w) + 2\Delta'(0^+)^2 \iint_w \Delta''(w)^2] I_q
\end{aligned}$$

FIG. 4. All diagrams correcting the disorder up to 3-loop order. All  $\Delta$  are bare  $\Delta_0$ , with the index suppressed for compactness of notation. While we calculated the corrections to  $\Delta(w)$ , we report its integrated form  $\delta R(w) := -\int_0^w dw' \int_0^{w'} dw'' \delta \Delta(w)$  for compactness. This is the correction to the potential correlator  $R(w)$ . The nonunderlined terms are present in the statics [66]; the underlined ones are additional contributions at depinning. We note that the following expressions are proportional to each other:  $(o) \sim (l)$  and  $(h) \sim (j)$ . The momentum integrals, which correspond to the icons in the same line, are given in Appendix A.

This yields the  $\beta$  function for the renormalized dimensionless disorder  $\tilde{\Delta}(w)$ :

$$\begin{aligned} \partial_\ell \tilde{\Delta}(w) = & (\epsilon - 2\zeta)\tilde{\Delta}(w) + \zeta w \tilde{\Delta}'(w) - \partial_w^2 \left\{ \frac{1}{2} [\tilde{\Delta}(0) - \tilde{\Delta}(w)]^2 \right\} \\ & - \partial_w^2 \left( \left( -\frac{1}{2} - \frac{\epsilon}{4} + C_3 \epsilon \right) \{ \tilde{\Delta}'(0^+)^2 \tilde{\Delta}(w) + [\tilde{\Delta}(w) - \tilde{\Delta}(0)] \tilde{\Delta}'(w)^2 \} \right) \\ & - \partial_w^2 \left( \frac{3}{4} \zeta (3) [\tilde{\Delta}'(w)^4 - 2 \tilde{\Delta}'(0^+)^2 \tilde{\Delta}'(w)^2 + 8 \tilde{\Delta}'(0^+)^2 \tilde{\Delta}''(0) \tilde{\Delta}(w)] \right. \\ & \left. + 2 \tilde{\Delta}'(w)^2 \{ \tilde{\Delta}'(0^+)^2 + [\tilde{\Delta}(w) - \tilde{\Delta}(0)] \tilde{\Delta}''(w) \} \right. \\ & \left. + C_3 \left\{ [\tilde{\Delta}(w) - \tilde{\Delta}(0)]^2 \tilde{\Delta}''(w)^2 - \frac{1}{2} \tilde{\Delta}'(w)^4 + [\tilde{\Delta}(0) - \tilde{\Delta}(w)] \tilde{\Delta}'(w)^2 \tilde{\Delta}''(w) - 6 \tilde{\Delta}'(0^+)^2 \tilde{\Delta}''(0) \tilde{\Delta}(w) \right\} \right) \\ & + 2 \tilde{\Delta}'(0^+)^2 \tilde{\Delta}''(w)^2 + O(\tilde{\Delta}^5), \end{aligned} \quad (40)$$

$$C_3 = \frac{\psi'(\frac{1}{3})}{6} - \frac{\pi^2}{9}. \quad (41)$$

The first two terms are a consequence of the rescaling Eq. (39), while the remaining ones are the direct loop corrections: The 1-loop term is on the first line, the 2-loop terms on the second line, followed by the 3-loop contributions.

Let us compare this  $\beta$  function to the 3-loop result in equilibrium, obtained in Ref. [66]. We see that the flow equations differ by anomaly terms [terms proportional to  $\Delta'(0^+)^2$ ]. All additional terms (at depinning, as compared with equilibrium) are underlined in Fig. 4. Let us already point out that, in equilibrium, the random-field (RF) fixed point (FP) discussed in the next section has a trivial exponent of  $\zeta = \epsilon/3$  to all orders.

### B. Fixed point

Equation (40) has a discrete set of fixed points (FP), among which one is fully attractive and represents the dominant random-field universality class, see, e.g., Ref. [33]. While we could in principle follow the flow to this attractive fixed point, it is better to directly write down the fixed-point equation, which gives  $\zeta$  and  $\tilde{\Delta}(w)$  to 3-loop order. While at 1-loop order we can do this analytically, much of the information for 2-loop and 3-loop order must be obtained numerically. Useful analytic constraints are obtained by integrating Eq. (40) over  $w$ :

$$\begin{aligned} 0 = & \int_0^\infty \partial_\ell \tilde{\Delta}(w) dw \\ = & (\epsilon - 3\zeta) \int_0^\infty \tilde{\Delta}(w) dw - \left( 1 - 2C_3 \epsilon + \frac{\epsilon}{2} \right) \tilde{\Delta}'(0^+)^3 \\ & + 3[2 - 3C_3 + 2\zeta(3)] \tilde{\Delta}'(0^+)^3 \tilde{\Delta}''(0) \\ & + 2 \tilde{\Delta}'(0^+)^2 \int_0^\infty \tilde{\Delta}''(w)^2 dw. \end{aligned} \quad (42)$$

We used that  $\tilde{\Delta}(w)$  is decaying fast to zero for  $w \rightarrow \infty$ ; thus, all boundary terms at infinity vanish. Here,  $\lim_{w \rightarrow \infty} w \tilde{\Delta}(w) = \lim_{w \rightarrow \infty} \tilde{\Delta}'(w) = \dots = 0$ . We make the ansatz

$$\tilde{\Delta}(w) = \frac{\epsilon}{3} y(w) + \frac{\epsilon^2}{18} y_2(w) + \epsilon^3 y_3(w), \quad (43)$$

$$\zeta = \frac{\epsilon}{3} + \zeta_2 \epsilon^2 + \zeta_3 \epsilon^3 + \dots, \quad (44)$$

$$y(0) = 1, \quad y_2(0) = 0, \quad y_3(0) = 0. \quad (45)$$

(The numerical factors  $\frac{1}{3}$  and  $\frac{1}{18}$  are for historical reasons, to agree with the conventions of Ref. [47]).

### C. 1-loop order

After integrating the 1-loop solution twice, this yields (see, e.g., Ref. [33], sec. 2.6)

$$\frac{w^2}{2} - y(w) + \ln(y(w)) + 1 = 0. \quad (46)$$

This is a simple expression for  $w(y)$ . Mathematica knows the inverse function  $y(w)$  as a ProductLog:

$$y(w) = -W \left( -\exp \left( -\frac{w^2}{2} - 1 \right) \right). \quad (47)$$

Its series expansion is

$$\begin{aligned} y(w) = & 1 - w + \frac{w^2}{3} - \frac{w^3}{36} - \frac{w^4}{270} - \frac{w^5}{4320} + \frac{w^6}{17010} \\ & + \frac{139w^7}{5443200} + \frac{w^8}{204120} + \frac{571w^9}{2351462400} \\ & - \frac{281w^{10}}{1515591000} + \dots \end{aligned} \quad (48)$$

Integrals we need later are

$$a_1 := \int_0^\infty dw y(w) = 0.7753042451883378, \quad (49)$$

$$a_2 := \int_0^\infty dw y''(w)^2 = 0.44750763980522135. \quad (50)$$

Simple analytical integral representations are obtained by converting the  $w$  integrals into  $y$  integrals:

$$a_1 = \sqrt{2} \int_0^1 \sqrt{y - \ln(y) - 1} dy, \quad (51)$$

$$\begin{aligned} a_2 = & \frac{2}{3} + \sqrt{2} \int_0^1 \frac{y \sqrt{y - \ln(y) - 1}}{(y-1)^5} \\ & \times [(y-1)(y+5) - 2(2y+1) \ln(y)] dy. \end{aligned} \quad (52)$$

**D. 2-loop order**

As a first consequence of the integral relation in Eq. (42), we find to order  $\epsilon^2$

$$-\zeta_2 \int_0^\infty y(w) dw - \left[ \frac{y'(0)}{3} \right]^3 = 0. \tag{53}$$

Equation (42) at 2-loop order then yields

$$\begin{aligned} \zeta_2 &= \frac{1}{27a_1} = 0.047\,770\,971\,546\,823\,057\,794\,614\,541\,634\,509\,315\,938\,52 \\ &= \frac{0.143\,312\,914\,640\,469\,173\,383\,843\,624\,903\,527\,947\,815\,6}{3}. \end{aligned} \tag{54}$$

We then need  $y_2(w)$ . A good approximation is obtained by solving the 2-loop  $\beta$  function perturbatively around 0 and then producing a fit for  $y_2(w)/y(w)^2$ :

$$\begin{aligned} y_2(w) &\approx (-1.140\,12w - 1.312\,45w^2 - 0.927\,184w^3 \\ &\quad - 0.509\,678w^4 - 0.237\,76w^5 - 0.098\,335\,7w^6 \\ &\quad - 0.037\,020\,5w^7 - 0.012\,913\,5w^8 \\ &\quad - 0.004\,228\,06w^9 \\ &\quad - 0.001\,312\,26w^{10} + \dots)y(w)^2. \end{aligned} \tag{55}$$

A second approximation stems from the observation that  $y_2(w) \approx \text{const. } wy'(w)$ , which would arise when the second-order solution just changes its amplitude, and this amplitude change is absorbed via a rescaling, sending  $w \rightarrow w[1 + O(\epsilon)]$ . We can therefore write (with more terms used in practice)

$$y_2(w) \approx [1.140\,12 + O(w)]wy'(w). \tag{56}$$

Another approximation is to do a Taylor expansion on  $y_2(w)/[wy'(w)]$  and then use the diagonal Padé for its approximation. We show for illustration a relative low-order approximant:

$$\begin{aligned} y_2(w) &= \frac{1.140\,12 - 0.597\,926w + 0.093\,139\,3w^2 + \dots}{1 - 0.342\,252w + 0.046\,522\,1w^2 + \dots} \\ &\quad \times wy'(w). \end{aligned} \tag{57}$$

Later, we need

$$a_3 := \int_0^\infty y_2(w) dw = -0.636\,336(1 \pm 7 \times 10^{-5}). \tag{58}$$

The error bar is from a numerical solution of the FP equation combined with the approximations in Eqs. (55)–(57).

**E. 3-loop order**

The integral relation in Eq. (42) to next order reads

$$\begin{aligned} 0 &= -\zeta_3 a_1 - \frac{\zeta_2}{6} a_3 \\ &\quad - \left( -2C_3 + \frac{1}{2} \right) \frac{y'(0)^3}{3^3} - 3 \frac{y'(0)^2}{3^2} \frac{y_2'(0)}{18} \end{aligned}$$

$$\begin{aligned} &+ 3[2 - 3C_3 + 2\zeta(3)] \frac{y'(0)^3}{3^3} \frac{y''(0)}{3} \\ &+ 2 \frac{y'(0)^2}{3^2} \frac{a_2}{3^2}. \end{aligned} \tag{59}$$

Inserting everything we calculated above, we find [78]

$$\zeta_3 = \begin{cases} -0.068\,354\,5 & \text{from Eq. (55) at order 30,} \\ -0.068\,354\,7 & \text{from Eq. (55) at orders 30–40,} \\ -0.068\,354\,36 & \text{from Eq. (56) at order 30,} \\ -0.068\,354\,414 & \text{from Eq. (57) from Padé}_{15,15}, \\ -0.068\,354\,4 & \text{with } a_3 \text{ from shooting for } y_2(w). \end{cases} \tag{60}$$

Solving the  $\beta$  function numerically via shooting, we find

$$\zeta_3 = -0.068\,354\,4. \tag{61}$$

This value is especially consistent with the last value in Eq. (60). The relative difference of the above values is better than  $10^{-5}$ .

We can also create a series expansion for  $y_3(w)$ , as we did for  $y_2(w)$ . Doing this and using shooting with  $\Delta(w = 4) = 0$  [instead of  $\Delta(\infty) = 0$ ], we find (probably less reliable)

$$\zeta_3 = -0.068\,380\,3. \tag{62}$$

Neglecting this last value, our confidence for  $\zeta_3$  is

$$\zeta_3 = -0.068\,354\,4(2). \tag{63}$$

**F. Numerical values and resummation**

Figure 5 shows both the direct sum as well as various approximations. From the various Padé approximants, the best one is Padé<sub>2,1</sub>:

$$\zeta(\epsilon) \approx \epsilon \frac{\frac{1}{3} + 0.524\,731\epsilon}{1 + 1.430\,88\epsilon} + O(\epsilon^4). \tag{64}$$

It is the only Padé approximant which is monotone for large  $\epsilon$ .

A similar approximant can be used for a Padé-Borel resummation. To this aim, we define

$$\zeta^{\text{Borel}}(t) := \sum_{n=1}^\infty \frac{\zeta_n t^n}{n!}. \tag{65}$$

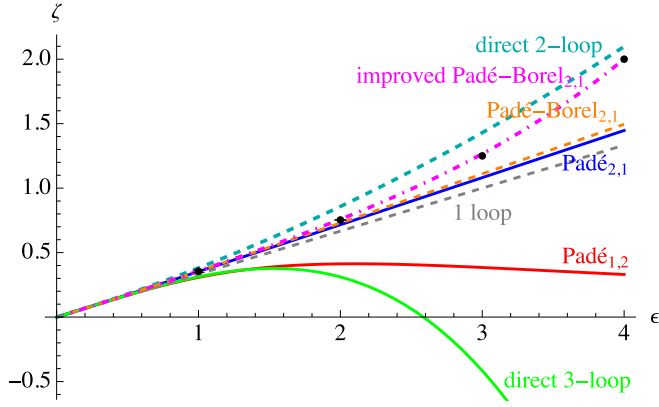


FIG. 5.  $\zeta(\epsilon)$  in different schemes: 1-loop (black, dashed), direct 2-loop (cyan), direct 3-loop (green), as well as two Padé approximants:  $\text{Padé}_{1,2}$  (red) and  $\text{Padé}_{2,1}$  (blue). For the latter, we also show the Padé-Borel resummation as explained in the main text. The black dots are the result of numerical simulations for  $d = 2, 3$ , and the exact values  $\zeta = \frac{5}{4}$  in  $d = 1$  as well as  $\zeta = 2$  in  $d = 0$ .

This series stops at order  $t^3$  (3-loop order). As above, the Padé approximant which behaves well for large  $t$  is  $\text{Padé}_{2,1}$ :

$$\zeta_{\text{Padé}_{2,1}}^{\text{Borel}}(t) = \frac{\frac{t}{3} + 0.182872t^2}{1 + 0.47696t}. \quad (66)$$

Using this, we obtain an approximation [79] for  $\zeta$ :

$$\zeta^{\text{Padé-Borel}}(\epsilon) := \int_0^\infty \frac{dt}{\epsilon} \zeta_{\text{Padé}_{2,1}}^{\text{Borel}}(t) \exp\left(-\frac{t}{\epsilon}\right). \quad (67)$$

Let us use this as a reference for the best 3-loop approximation. We remark that, in  $d = 3$ , there is a marked improvement, and the  $\epsilon$ -expansion result is now spot on the numerical solution, probably even more precise than the latter. In  $d = 2$ , the improvement in precision is also noticeable, with a relative deviation of  $<4\%$ . In  $d = 1$ , the relative error is now at 12%, while  $d = 0$  is out of reach.

To improve the precision, we can use the information in  $d = 0$ , where  $\zeta = 2$  (with  $\sqrt{\ln}$  corrections); this fixes the

TABLE I. Comparison of the various approximations for  $\zeta$  and numerical values.

Method	$d = 0$	$d = 1$	$d = 2$	$d = 3$
Numeric/exact	2	$\frac{5}{4}$	0.753(2)	0.355(10)
1-loop	$\frac{4}{3}$	1	$\frac{2}{3}$	$\frac{1}{3}$
Direct 2-loop	2.097 67	1.429 94	0.857 75	0.381 10
Direct 3-loop	-2.277 02	-0.415 63	0.310 92	0.312 75
$\text{Padé}_{1,2}$	0.330 33	0.384 54	0.412 60	0.307 99
$\text{Padé}_{2,1}$	1.447 01	1.081 23	0.716 15	0.352 99
$\text{Padé-Borel}_{2,1}$	1.478 06	1.100 53	0.725 39	0.355 12
Improved	2	1.265 67	0.753 41	0.357 16
Twice improved	2	1.25	0.751 82	0.356 58

coefficient of an additional quartic term:

$$\zeta^{\text{improved}}(\epsilon) = \zeta^{\text{Padé-Borel}}(\epsilon) + 0.002\,038\,84\epsilon^4. \quad (68)$$

With this correction, the prediction in  $d = 1$  becomes 1.266, very close to the analytically known value of  $\zeta = \frac{5}{4}$  [80]. Using in addition  $\zeta(d = 1) = \frac{5}{4}$ , we find

$$\zeta^{\text{twice improved}}(\epsilon) = \zeta^{\text{Padé-Borel}}(\epsilon) + 0.001\,264\,88\epsilon^4 + 0.000\,193\,49\epsilon^5. \quad (69)$$

This is summarized in Table I. Our best predictions and error estimates for the unknown dimensions  $d = 2$  and 3 thus are

$$\zeta_{d=2}^{\text{best}} = 0.752(1), \quad (70)$$

$$\zeta_{d=3}^{\text{best}} = 0.357(1). \quad (71)$$

### G. The $\beta$ function in minimal subtraction

The minimal subtraction scheme takes a prominent role in high-order RG calculations. How can this be implemented here? The idea is to make an ansatz for  $\Delta_r(w)$  as a functional of  $\Delta_0(w)$  and then to write the effective  $\Delta_{\text{eff}}(w)$  in Eq. (36) as a function of  $\Delta_r(w)$ , keeping only singular terms (minimal subtraction). Since  $\Delta_{\text{eff}}(w)$  is an observable, it must be finite when expressed in terms of  $\Delta_r(w)$ . This uniquely fixes  $\Delta_r(\Delta_0)$ . Let us make the ansatz:

$$\begin{aligned} \Delta_r(w) &= \Delta_0(w) + \delta^{(1)}\Delta(w) + \mathcal{S} \circ \delta^{(2)}\Delta(w) + \delta^{(3)}\Delta(w) \\ &+ \frac{1}{8}(\mathcal{F} \circ I_A)I_1(7[\Delta_0(w) - \Delta_0(0)]\Delta_0'(w)^2\Delta_0''(w) + \Delta_0'(0)^2\{6\Delta_0''(0)\Delta_0(w) + [\Delta_0(w) - \Delta_0(0)]\Delta_0''(w)\}) \\ &+ \Delta_0'(w)^4 + 2[\Delta_0(0) - \Delta_0(w)]^2\Delta_0^{(3)}(w)\Delta_0'(w) + \dots \end{aligned} \quad (72)$$

Here,  $\mathcal{S}$  extracts the singular (in  $\epsilon$ ) part of a diagram, while  $\mathcal{F}$  extracts its finite part  $(\mathcal{S} + \mathcal{F}) \circ I \equiv I$ . The expression in big parentheses is what is obtained if one inserts the 1-loop expression into the 2-loop expression (repeated counterterm). This operation is successful, as

$$\Delta_{\text{eff}}(w) = \Delta_r(w) + \frac{4C_3 - 1}{8}(2[\Delta_r(0) - \Delta_r(w)]\Delta_r'''(w)\Delta_r'(w) - \Delta_r''(w)\{\Delta_r'(0)^2 + 5\Delta_r'(w)^2 + 2[\Delta_r(w) - \Delta_r(0)]\Delta_r''(w)\}). \quad (73)$$



The ensuing  $\beta$  function is longer than that in Eq. (40), and we refrain from putting it here. It is more interesting to look at the difference:

$$\begin{aligned} \partial_\ell \tilde{\Delta}(w) - \partial_\ell \Delta_r(w)|_{\Delta_r=\tilde{\Delta}} &= -\frac{4C_3-1}{4} \partial_w^2 \{ \epsilon [\tilde{\Delta}(0) - \tilde{\Delta}(w)] [\tilde{\Delta}'(0)^2 + \tilde{\Delta}'(w)^2] \} \\ &\quad - \frac{4C_3-1}{8} \partial_w^2 (\tilde{\Delta}'(w)^4 + 2[\tilde{\Delta}(w) - \tilde{\Delta}(0)] \tilde{\Delta}'(w)^2 \tilde{\Delta}''(w) \\ &\quad + 2[\tilde{\Delta}(0) - \tilde{\Delta}(w)] \{ [\tilde{\Delta}(w) - \tilde{\Delta}(0)] \tilde{\Delta}''(w)^2 - 6\tilde{\Delta}'(0^+)^2 \tilde{\Delta}''(0) \}). \end{aligned} \quad (74)$$

A consistency check is that this yields the same  $\zeta_3$ . Integrating this equation over all  $w$  yields

$$\int_0^\infty \partial_\ell \tilde{\Delta}(w) - \partial_\ell \Delta_r(w)|_{\Delta_r=\tilde{\Delta}} dw = \frac{4C_3-1}{2} \epsilon \tilde{\Delta}'(0^+)^3 + \frac{9(1-4C_3)}{4} \tilde{\Delta}'(0^+)^3 \tilde{\Delta}''(0). \quad (75)$$

Using Eqs. (43) and (48) shows that this vanishes at the required order  $\epsilon^4$ . Thus,  $\zeta$  is independent of the scheme up to 3-loop order.

#### IV. THE CRITICAL FORCE

While renormalization of the disorder was already considered in the original 2-loop calculation [46,47], the dependence of the critical force at depinning was only considered in simulations [62] but not via RG. Here, we address this issue. We give explicit results for each of the dynamic diagrams involved up to 2-loop order.

##### A. 1 loop

The diagram in question is

$$\begin{aligned} \begin{array}{c} \xleftarrow{t_2} \\ \bullet \\ \vdots \\ \bullet \\ \xrightarrow{x} \\ t_1 \end{array} &= \tilde{u}(x, t_2) \int_{t_1, k} \Delta'_0(u(x, t_2) - u(x, t_1)) \exp(-(t_2 - t_1)(k^2 + m^2)) \Theta(t_1 < t_2) \\ &\simeq \tilde{u}(x, t_2) \int_{t_1, k} [\Delta'_0(0^+) + \Delta''_0(0^+)(t_2 - t_1) \dot{u}(x, t_2) + \dots] \exp(-(t_2 - t_1)(k^2 + m^2)) \Theta(t_1 < t_2) \\ &= \tilde{u}(x, t_2) \int_k \frac{\Delta'_0(0^+)}{k^2 + m^2} + \frac{\Delta''_0(0^+)}{(k^2 + m^2)^2} \dot{u}(x, t_2) + \dots \end{aligned} \quad (76)$$

The first term is the correction to the critical force, the second term the correction to friction. In summary,

$$\delta f_c^{(1)} = \Delta'(0^+) I_{\text{tp}}, \quad (77)$$

$$I_{\text{tp}} = \textcircled{\bullet} = \int_k \frac{1}{k^2 + m^2} = \frac{2m^2}{(d-4)(d-2)} (\epsilon I_1). \quad (78)$$

See Appendix A 2 for the integral.

##### B. 2 loop

At 2-loop order, there are seven contributions to the critical force. Including all combinatorial factors, these read

$$\delta^{(2)} f_c = \mathcal{F}_1 + \mathcal{F}_2 + \mathcal{F}_3 + \mathcal{F}_4 + \mathcal{F}_5 + \mathcal{F}_6 + \mathcal{F}_7, \quad (79)$$

$$\mathcal{F}_1 = \begin{array}{c} \bullet \xrightarrow{\quad} \bullet \\ \vdots \quad \quad \vdots \\ \bullet \xrightarrow{\quad} \bullet \\ \vdots \quad \quad \vdots \\ \bullet \xrightarrow{\quad} \bullet \end{array} = -\Delta''(0) \Delta'(0^+) I_{\text{ss}} \quad (80)$$

$$\mathcal{F}_2 = \begin{array}{c} \bullet \xrightarrow{\quad} \bullet \\ \vdots \quad \quad \vdots \\ \bullet \xrightarrow{\quad} \bullet \\ \vdots \quad \quad \vdots \\ \bullet \xrightarrow{\quad} \bullet \end{array} = -\Delta(0) \Delta'''(0^+) I_1 I_{\text{tp}} \quad (81)$$

$$\mathcal{F}_3 = \begin{array}{c} \bullet \xrightarrow{\quad} \bullet \\ \vdots \quad \quad \vdots \\ \bullet \xrightarrow{\quad} \bullet \\ \vdots \quad \quad \vdots \\ \bullet \xrightarrow{\quad} \bullet \end{array} = 0 \quad (\text{see below}) \quad (82)$$

$$\mathcal{F}_4 = \begin{array}{c} \bullet \xrightarrow{\quad} \bullet \\ | \quad \quad | \\ \bullet \xleftarrow{\quad} \bullet \end{array} = -\Delta'(0^+)\Delta''(0)I_1I_{\text{tp}} \quad (83)$$

$$\mathcal{F}_5 = \frac{1}{2} \begin{array}{c} \bullet \xrightarrow{\quad} \bullet \\ | \quad \quad | \\ \bullet \xrightarrow{\quad} \bullet \end{array} = \frac{1}{2}\Delta(0)\Delta'''(0^+)I_1I_{\text{tp}} \quad (84)$$

$$\mathcal{F}_6 = \frac{1}{2} \begin{array}{c} \bullet \xrightarrow{\quad} \bullet \\ | \quad \quad | \\ \bullet \xrightarrow{\quad} \bullet \end{array} = \frac{1}{2}\Delta(0)\Delta'''(0^+)I_1I_{\text{tp}} \quad (85)$$

$$\mathcal{F}_7 = \begin{array}{c} \bullet \xrightarrow{\quad} \bullet \\ | \quad \quad | \\ \bullet \xrightarrow{\quad} \bullet \end{array} = \Delta''(0)\Delta'(0^+)I_1I_{\text{tp}} \quad (86)$$

The nontrivial diagram  $\mathcal{F}_3$  is

$$\begin{aligned} \mathcal{F}_3 &= \Delta'(0^+)\Delta''(0^+) \int_{k,q} \int_{t_1,t_2,t_3} \exp(-k^2t_1 - (k+q)^2t_2 - q^2t_3 - m^2(t_1+t_2+t_3)) \text{sign}(t_3-t_1) \\ &= \int_{k,q} \frac{k^2 - q^2}{(k^2+m^2)(q^2+m^2)(k^2+q^2+2m^2)((k+q)^2+m^2)} = 0. \end{aligned} \quad (87)$$

Further cancelations read

$$\mathcal{F}_2 + \mathcal{F}_5 + \mathcal{F}_6 = 0, \quad \mathcal{F}_4 + \mathcal{F}_7 = 0. \quad (88)$$

Thus,

$$\sum_{i=1}^7 \mathcal{F}_i = \mathcal{F}_1 = -\Delta'(0^+)\Delta''(0)I_{\text{ss}}. \quad (89)$$

The sunset diagram  $I_{\text{ss}}$  reads

$$\begin{aligned} I_{\text{ss}} &= \begin{array}{c} \bullet \text{---} \bullet \\ \text{---} \text{---} \text{---} \\ \bullet \text{---} \bullet \end{array} \\ &= \int_{k,p} \frac{1}{(k^2+m^2)(p^2+m^2)[(k+p)^2+m^2]}. \end{aligned} \quad (90)$$

It is evaluated in Appendix A 4:

$$I_{\text{ss}} = m^2 \left[ -\frac{3}{2\epsilon^2} - \frac{9}{4\epsilon} - \frac{3(7-4C_3)}{8} + \dots \right] (\epsilon I_1)^2. \quad (91)$$

### C. 3 loop

At 3-loop order, there are nine diagrams, shown in Fig. 6. Diagram (r) reads

$$(r) = \Delta'(0^+) \left[ 3\Delta''(0)^2 + 2\Delta'''(0^+)\Delta'(0^+) \right] \begin{array}{c} \bullet \\ \diagup \quad \diagdown \\ \bullet \text{---} \bullet \\ \diagdown \quad \diagup \\ \bullet \end{array}. \quad (92)$$

The integral is calculated in Appendix A 9:

$$\begin{aligned} I_r &= \begin{array}{c} \bullet \\ \diagup \quad \diagdown \\ \bullet \text{---} \bullet \\ \diagdown \quad \diagup \\ \bullet \end{array} \\ &= m^2(\epsilon I_1)^3 \left[ -\frac{1}{\epsilon^3} - \frac{17}{6\epsilon^2} + \frac{36C_3 - 67}{12\epsilon} + \mathcal{O}(\epsilon^0) \right]. \end{aligned} \quad (93)$$

After some tedious calculations, one surprisingly finds that all remaining contributions vanish:

$$(s) = (t) = (u) = (v) = (w) = (x) = (y) = (z). \quad (94)$$

### D. Critical force to 3-loop order and flow equation

Up to UV-cutoff dependent terms,

$$\begin{aligned} f_c &= \Delta'_0(0^+)I_{\text{tp}} - \Delta'_0(0^+)\Delta''_0(0^+)I_{\text{ss}} \\ &\quad + [2\Delta'''_0(0)\Delta'_0(0)^2 + 3\Delta'_0(0)\Delta''_0(0)^2]I_r + \dots \end{aligned} \quad (95)$$

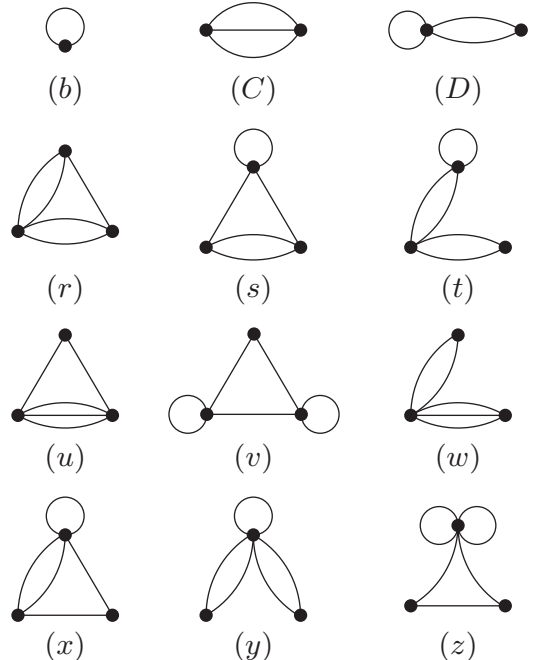


FIG. 6. All spatial diagrams for corrections of  $F_c$  and  $\eta$ ; the first three diagrams (without label) are the 1- and 2-loop contributions. The remaining nine diagrams (r) to (z) are 3-loop contributions.

The following flow is finite (the  $\Lambda$ -dependent terms have disappeared under the  $m$  variation):

$$\begin{aligned} & -m\partial_m(u-w) \\ & \equiv m\partial_m[f_c m^{-2}] \\ & = -\epsilon m^{-2} \{ \Delta'_0(0^+) I_{\text{tp}} - 2\Delta'_0(0^+) \Delta''_0(0^+) I_{\text{ss}} \\ & \quad + 3[2\Delta'''_0(0) \Delta'_0(0)^2 + 3\Delta'_0(0) \Delta''_0(0)^2] I_r + O(\Delta_0^4) \}. \end{aligned} \quad (96)$$

The following step is to replace  $\Delta_0(w)$  by  $\Delta_{\text{eff}}(w)$  using Eq. (38). In the next step, we use a generalization of Eq. (39):

$$\Delta_{\text{eff}}(w) = \frac{m^{-2\zeta}}{\epsilon I_1 \lambda^2} \tilde{\Delta}(\lambda w m^\zeta). \quad (97)$$

The factor of  $\lambda$  is a number which can be chosen freely due to the invariance of the  $\beta$  function under this rescaling. [The reader can easily check that  $\tilde{\Delta}(w)$  solves the RG flow Eq. (40), independently of  $\lambda$ .] Here,  $\lambda$  is fixed by the experiment or simulation. The easiest way to achieve this is to divide Eq. (97) by its first  $w$  derivative:

$$\frac{m^{-\zeta}}{\lambda} \frac{\tilde{\Delta}(0)}{|\tilde{\Delta}'(0^+)|} = \frac{\Delta_{\text{eff}}(w)}{|\Delta'_{\text{eff}}(w)|} =: \rho_m. \quad (98)$$

The scale  $\rho_m$  is the correlation length of the effective disorder in the driving direction, measured in Sec. VI. Equation (98)

can be written as

$$\frac{m^{-\zeta}}{\lambda} = \frac{\rho_m}{\tilde{\rho}}, \quad \tilde{\rho} := \frac{\tilde{\Delta}(0)}{|\tilde{\Delta}'(0^+)|}. \quad (99)$$

The last combination  $\tilde{\rho}$  is a theoretical object, depending on the choice of scheme to solve the FRG equation, see the ansatz in Eq. (43). Using Eq. (99) to eliminate  $\lambda$ , we rewrite Eq. (97) as

$$\Delta_{\text{eff}}(w) = \frac{\rho_m^2}{\epsilon I_1} \tilde{\Delta}\left(\frac{w}{\rho_m}\right). \quad (100)$$

For the perturbative calculation of  $f_c$ , there are two important points: First, the integrals  $I_{\text{tp}}$ ,  $I_{\text{ss}}$ , and  $I_r$  can be combined into the dimensionless combinations:

$$\frac{I_{\text{tp}}}{m^2 \epsilon I_1} = \frac{2}{(\epsilon - 2)\epsilon}, \quad (101)$$

$$\frac{I_{\text{ss}}}{m^2 (\epsilon I_1)^2} = -\frac{3}{2\epsilon^2} - \frac{9}{4\epsilon} - \frac{3}{8}(7 - 4C_3) + \dots, \quad (102)$$

$$\frac{I_r}{m^2 (\epsilon I_1)^3} = -\frac{1}{\epsilon^3} - \frac{17}{6\epsilon^2} + \frac{36C_3 - 67}{12\epsilon} + \dots \quad (103)$$

Second, a global factor of  $m^{-\zeta}/\lambda = \rho_m/\tilde{\rho}$  appears from the single  $\Delta'(0^+)$ , whereas  $\Delta''(0)$  and  $\Delta'(0^+)\Delta'''(0^+)$  do not give additional factors of  $m^{\pm\zeta}$  or  $\lambda$ . Therefore, Eq. (96), expressed in terms of the renormalized dimensionless disorder  $\tilde{\Delta}$  and scales  $m$  and  $\rho$ , reads

$$\begin{aligned} m\partial_m[f_c m^{-2}] & = \frac{2}{2-\epsilon} \frac{m^{-\zeta}}{\lambda} \{ -\tilde{\Delta}'(0^+) + 3\tilde{\Delta}'(0^+)\tilde{\Delta}''(0)[1 + \epsilon(1-C_3) + \dots] \\ & \quad + (C_3-6)\tilde{\Delta}'(0^+)[3\tilde{\Delta}''(0)^2 + 2\tilde{\Delta}'''(0)\tilde{\Delta}'(0^+)] + \dots + O(\tilde{\Delta}^4) \} \\ & = \tilde{\mathcal{A}} \frac{m^{-\zeta}}{\lambda} = \tilde{\mathcal{A}} \frac{\rho_m}{\tilde{\rho}}. \end{aligned} \quad (104)$$

We grouped all terms for a given loop order in the same line and expanded as far as necessary in  $\epsilon$ . Inserting the RF fixed point, we find

$$\begin{aligned} \tilde{\mathcal{A}} & = \frac{2}{2-\epsilon} \{ -\tilde{\Delta}'(0^+) + 3\tilde{\Delta}'(0^+)\tilde{\Delta}''(0)[1 + \epsilon(1-C_3) + \dots] \\ & \quad + (C_3-6)\tilde{\Delta}'(0^+)[3\tilde{\Delta}''(0)^2 + 2\tilde{\Delta}'''(0)\tilde{\Delta}'(0)] + \dots + O(\tilde{\Delta}^4) \} \\ & = \frac{\epsilon}{3} + 0.007784584\epsilon^2 + 0.0170387\epsilon^3 + O(\epsilon^4). \end{aligned} \quad (105)$$

To solve Eq. (104), we use that  $\rho_m \sim m^{-\zeta}$ , to obtain

$$\frac{f_c}{m^2} = -\frac{\tilde{\mathcal{A}}}{\zeta} \frac{\rho_m}{\tilde{\rho}} + m\text{-independent term}. \quad (106)$$

This is equivalent to

$$f_c = f_0 - \mathcal{B} \rho_m m^2 + O(m^2), \quad (107)$$

$$\mathcal{B} := \frac{\tilde{\mathcal{A}}}{\zeta \tilde{\rho}} = 1 + 0.070061\epsilon + 0.0127138\epsilon^2 + O(\epsilon^3), \quad (108)$$

$$\tilde{\rho} = 1 - 0.190020\epsilon + 0.27397\epsilon^2 + O(\epsilon^3). \quad (109)$$

This is plotted on Fig. 7. Note that we added a term  $f_0 \sim \Lambda^{d-2} \Delta'_0(0^+)$  due to the leading UV divergence of the tadpole diagram in Eq. (C5) which diverges with the UV cutoff  $\Lambda$

as  $\Lambda^{d-2}$  times the bare  $\Delta'_0(0^+)$ ; since this is a strong UV divergence, we used  $\Delta'(0^+)$  at the start of the RG flow, i.e., the microscopic  $\Delta'_0(0^+)$ .

We tried resummations for  $\tilde{\mathcal{A}}$ ,  $\mathcal{B}$ , and  $\zeta \mathcal{B} \equiv \tilde{\mathcal{A}}/\tilde{\rho}$ . The series for  $\mathcal{B}$  has only positive terms; thus, the result increases at each order, and we do not know how to resum. The combination  $\zeta \mathcal{B}$  reported in Fig. 8 is alternating, and both the diagonal Padé resummation and the diagonal Padé-Borel resummation lie close to each other and the 1-loop result. We report all 3-loop values in Table II. The prediction for  $\mathcal{B}$  from the extrapolation of  $\zeta \mathcal{B}$  uses the best numerically available values for  $\zeta$ .

We tried to improve the extrapolation by linking to the exactly known critical force in dimension  $d = 0$ . As can be

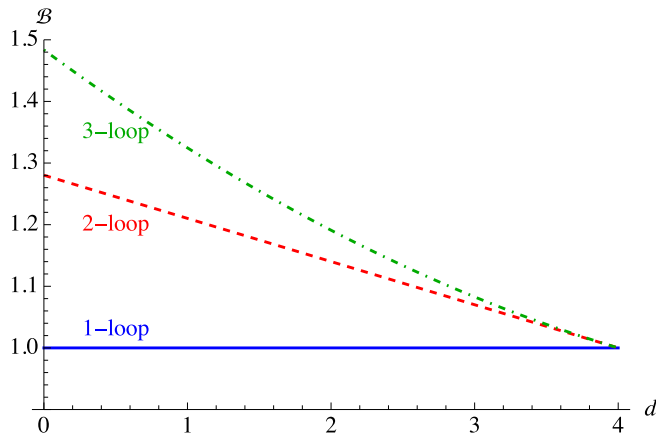


FIG. 7. The amplitude  $\mathcal{B}$  in Eq. (108). 1-loop (blue solid), 2-loop (red, dashed), and 3-loop (green, dot-dashed).

seen in Appendix D, there is an additional  $\ln m$  divergence which prevents us from exploiting this result.

## V. CRITICAL FORCE FOR CDWs

### A. Summary of known results

In Refs. [30,81], it was shown that CDWs at depinning map onto the  $O(n)$  model in the limit of  $n \rightarrow -2$ . The latter further maps onto loop-erased random walks [30,81–83]. The dynamic exponent  $z$  in CDWs equals the fractal dimension of loop-erased random walks. In  $\phi^4$  theory, this fractal dimension is given by the dimension of the traceless rank-2 tensor:

$$\mathcal{T}^{ij} = \phi^i \phi^j - \delta^{ij} \frac{1}{n} \sum_{k=1}^n (\phi^k)^2. \quad (110)$$

An interesting question is whether the critical force also has a representation in  $\phi^4$  theory. We show below that this is the case, and the critical force formally behaves as a logarithmic operator in a log-CFT.

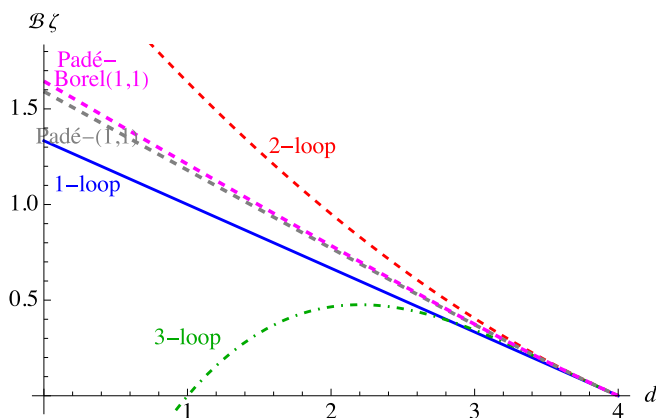


FIG. 8. The combination  $\mathcal{B}\zeta \equiv \tilde{\mathcal{A}}/\tilde{\rho}$ . 1-loop (blue solid), 2-loop (red, dashed), and 3-loop (green, dot-dashed).

TABLE II. Values for  $\mathcal{B}$  using either a direct resummation of  $\mathcal{B}$  in Eq. (108) (first line) or the combination  $\zeta\mathcal{B}$  (second), which is then divided by the numerically known value of  $\zeta$  (third line). The fourth line is an estimate, based on the trend of the direct extrapolation, and our lack of confidence in the precision of the results. For the numerical value see Sec. VID.

	$d = 1$	$d = 2$	$d = 3$	$d = 4$
$\mathcal{B}$ (direct)	1.32	1.19	1.08	1
$\zeta\mathcal{B}$ (Padé-Borel)	1.21	0.78	0.374	0
$\mathcal{B}$ (using $\zeta\mathcal{B}$ )	0.96	1.036	1.048	1
$\mathcal{B}$ (estimate and error bars)	1.3(4)	1.1(1)	1.06(2)	1
$\mathcal{B}$ (numerics)	1.8(2)	–	–	–

### B. Critical force for CDWs

We first consider the CDW side. Following the conventions of Ref. [81], we parameterize the disorder-force correlator  $\Delta(u)$  for CDWs as

$$\Delta(u) = \Delta(0) - \frac{g}{2}u(1-u). \quad (111)$$

The fixed point for the  $\beta$  function in Eq. (40) is

$$\Delta(0) = \frac{\epsilon}{36} + \frac{\epsilon^2}{108} - \frac{\epsilon^3}{648}(1 + 18C_3) + O(\epsilon^4), \quad (112)$$

$$g = \frac{\epsilon}{3} + \frac{2\epsilon^2}{9} + \frac{\epsilon^3}{9}[1 - 2C_3 - 2\zeta(3)] + O(\epsilon^4). \quad (113)$$

Thus,  $\Delta'''(0^+) = 0$ , and Eq. (95) for the critical force simplifies to

$$f_c = \frac{g}{2} \text{ (loop)} - \frac{g^2}{2} \text{ (loop)} + \frac{3}{2}g^3 \text{ (loop)} + \dots \quad (114)$$

### C. $\Gamma^{(2)}$ as a function of $n$

The vector  $\phi^4$  theory related to CDWs is [81]

$$\mathcal{S}[\vec{\phi}] = \int_x \frac{1}{2}[\vec{\phi}(x)^2] + \frac{m^2}{2}\vec{\phi}(x)^2 + \frac{g}{8}[\vec{\phi}(x)^2]^2. \quad (115)$$

In these conventions, comparable quantities are related, e.g., the coupling constants  $g$  in Eqs. (111) and (115) are identical. Using the same RG scheme, also all RG functions, and the coupling at the fixed point given in Eq. (113) are identical. In this framework, we now evaluate the effective action  $\Gamma[\phi] = \frac{m^2}{2}\phi^2 + O(g)$ , equivalent to  $\Gamma^{(2)} = m^2 + O(g)$ . The result up to 4-loop order reads

$$\Gamma^{(2)} - m^2 = -\frac{g(n+2)}{2} \text{ (loop)} \quad (116)$$

$$\begin{aligned}
 & + \frac{g^2(n+2)^2}{4} \text{ (loop with two vertices)} + \frac{g^2(n+2)}{2} \text{ (loop with one vertex)} \\
 & - \frac{1}{8}g^3(n+2)^3 \text{ (triangle with one loop)} - \frac{1}{4}g^3(n+2)^2 \text{ (triangle with two loops)} \\
 & - \frac{1}{8}g^3(n+2)^3 \text{ (triangle with three loops)} - \frac{1}{4}g^3(n+2)(n+8) \text{ (triangle with four loops)} \\
 & - \frac{3}{4}g^3(n+2)^2 \text{ (triangle with five loops)} \\
 & + \frac{1}{4}g^4(n+2)(5n+22) \text{ (square with two diagonals)} \\
 & + \frac{1}{8}g^4(n+2)(n^2+6n+20) \text{ (square with four loops)} \\
 & + \frac{1}{4}g^4(n+2)(5n+22) \text{ (square with three diagonals)} \\
 & + O[g^4, (n+2)^2]
 \end{aligned} \tag{117}$$

By inspection, one sees that  $f_c$  is related to the dominant contribution in the limit of  $n \rightarrow -2$ :

$$\begin{aligned}
 -\frac{\partial}{\partial n} \Gamma^{(2)} \Big|_{n=-2} &= \frac{g}{2} \text{ (loop with one vertex)} - \frac{g^2}{2} \text{ (loop with two vertices)} + \frac{3g^3}{2} \text{ (triangle)} \\
 & - 3g^4 \text{ (square with two diagonals)} - \frac{3g^4}{2} \text{ (square with four loops)} - 3g^4 \text{ (square with three diagonals)} \\
 & + O(g^5),
 \end{aligned} \tag{118}$$

where the 4-loop contribution was not checked at depinning. We conjecture that, to all orders in perturbation theory:

$$f_c = -\frac{\partial}{\partial n} \Gamma^{(2)} \Big|_{n=-2}. \tag{119}$$

We now use that

$$\Gamma^{(2)}(m) = \Gamma^{(2)}(1)m^{(1/\nu)+\eta}. \tag{120}$$

Since we retain the coefficient in front of  $\phi^2$ , the anomalous dimension  $\eta$  of the field is taken out. Equation (119) implies that

$$\begin{aligned}
 m\partial_m[f_c m^{-2}] &= -\frac{\partial}{\partial n} \left[ \frac{m\partial}{\partial m} \Gamma^{(2)}(1)m^{(1/\nu)+\eta-2} \right]_{n=-2} \\
 &= -\frac{\partial}{\partial n} \left[ \left( \frac{1}{\nu} + \eta - 2 \right) \Gamma^{(2)}(1)m^{(1/\nu)+\eta-2} \right]_{n=-2} \\
 &= -\frac{\partial}{\partial n} \left[ \frac{1}{\nu} + \eta \right]_{n=-2}.
 \end{aligned} \tag{121}$$

Let us see where these contributions come from in the RG. According to Ref. [84],

$$\frac{1}{\nu} + \eta = 2 + \gamma_1 \quad (\text{eq. (19) of Ref. [84]}), \tag{122}$$

$$\gamma_1 = \mu \partial_\mu \ln Z_1 \quad (\text{eq. (14) of Ref. [84]}), \tag{123}$$

$$\begin{aligned}
 \mathcal{S} &= \int_x Z_1 \frac{m^2}{2} \vec{\phi}(x)^2 + \frac{Z_2}{2} [\vec{\nabla} \phi(x)]^2 \\
 &+ Z_4 \frac{16\pi^2}{4!} g \mu^\epsilon [\vec{\phi}(x)^2]^2 \quad (\text{eq. (8) of Ref. [84]}).
 \end{aligned} \tag{124}$$

Thus,  $f_c$  is entirely given by the RG factor  $Z_1$  and does not invoke a renormalization of the field.

Let us finally use Eq. (121) and the 6-loop results of Ref. [85]:

$$\begin{aligned}
 m\partial_m[f_c m^{-2}] &= \frac{\epsilon}{6} + \frac{\epsilon^2}{36} + \frac{1}{72} [1 - 8\zeta(3)]\epsilon^3 + \frac{-70\zeta(3) + 2800\zeta(5) - 6\pi^4 + 25}{6480} \epsilon^4 \\
 &+ \left[ \frac{7\zeta(3)^2}{162} - \frac{115\zeta(3)}{3888} + \frac{29\zeta(5)}{648} - \frac{833\zeta(7)}{432} + \frac{5\pi^6}{8748} - \frac{7\pi^4}{77760} + \frac{7}{7776} \right] \epsilon^5 \\
 &+ \left[ \frac{344\zeta(3)^3}{729} + \frac{443\zeta(3)^2}{1296} + \frac{953}{486} \zeta(5)\zeta(3) + \frac{7\pi^4\zeta(3)}{9720} - \frac{305\zeta(3)}{23328} + \frac{1511\zeta(5)}{23328} - \frac{17815\zeta(7)}{46656} \right. \\
 &\left. + \frac{60451\zeta(9)}{6561} + \frac{697\zeta_{3,5}}{540} - \frac{168317\pi^8}{244944000} + \frac{47\pi^6}{489888} - \frac{23\pi^4}{93312} - \frac{5}{15552} \right] \epsilon^6 + O(\epsilon^7).
 \end{aligned} \tag{125}$$

We find that this agrees up to 3-loop order with the result obtained for depinning.

We finally need to resum this asymptotic series. A relevant dimension is  $d = 3$ , for which we find (with possibly strongly

underestimated error bars)

$$-\partial_n \left[ \frac{1}{\nu} + \eta \right]_{n=-2, \epsilon=1} = 0.1585(5) \tag{126}$$

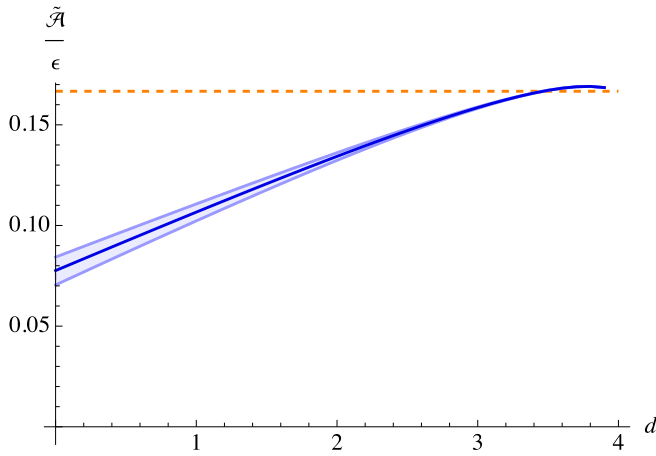


FIG. 9.  $\tilde{A}_c/\epsilon$  for charge density wave (CDW), given by Eq. (125). The error bars are probably an underestimation, as they do not catch the singularity at  $d = 2$ .

In dimension  $d = 2$ , we can try to use CFT data in Eq. (121). As we show in Appendix B 1, this expression diverges when taking the limit of  $n \rightarrow -2$ . We conjecture that, for  $d \leq 2$ , the critical force acquires an additional singularity not captured by the  $4 - \epsilon$  expansion. While our extrapolations are shown in Fig. 9 down to  $d = 0$ , we should thus not trust it for  $d \leq 2$ .

We saw above that the critical force for CDWs can be calculated in the  $O(n)$  model by deriving  $\Gamma^{(2)}$  with respect to  $n$ . This means that the operator in question is not living inside the theory at  $n = -2$  but in the larger set of theories around  $n = -2$ . This sometimes happens in log-CFTs. Here, we give one prescription to obtain  $f_c$  directly inside the theory at  $n = -2$ :

$$-\frac{g}{6}\phi_1(x)^3 e^{-S} \rightarrow f_c \phi_1(x). \quad (127)$$

This means, to evaluate the insertion  $-\frac{g}{6}\phi_1(x)^3$  inside the interacting field theory and retain the perturbative corrections proportional to  $\phi_1$ , their amplitude is  $f_c$ . This can be achieved by calculating the 2-point function of  $\phi_1(x)^3$ , with  $\phi_1(y)$ . The logic behind this and alternative constructions are discussed in Appendix B 2.

#### D. CDWs and log-CFT

We start this section with a reminder of logarithms in self-avoiding polymers [69]. The reader not familiar with the subject is invited to consult Appendix E or the original publication [69], where the math is worked out. The general idea is that there are two operators  $\mathcal{E}$  and  $\tilde{\mathcal{E}}$ , which at a critical value  $n_c$  of a control parameter  $n$  have the same full scaling dimension  $x_{\mathcal{E}}(n_c) = x_{\tilde{\mathcal{E}}}(n_c)$  and moreover become identical as operators. Approaching  $n_c$ , there are then two differences (or derivatives) one may consider: the difference between the operators  $\mathcal{E}$  and  $\tilde{\mathcal{E}}$  and the difference between their scaling dimensions  $x_{\mathcal{E}}(n) - x_{\tilde{\mathcal{E}}}(n)$ . It is a matter of conventions whether these differences vanish or are finite. If they vanish, we should divide by  $n - n_c$ , equivalent to taking a derivative. Let us write

the relations in the conventions of Appendix E, where the differences are finite. Define

$$\begin{aligned} \mathcal{C} &:= \lim_{n \rightarrow n_c} [x_{\mathcal{E}}(n) - x_{\tilde{\mathcal{E}}}(n)] \mathcal{E} \\ &\equiv \lim_{n \rightarrow n_c} [x_{\mathcal{E}}(n) - x_{\tilde{\mathcal{E}}}(n)] \tilde{\mathcal{E}}, \end{aligned} \quad (128)$$

$$\mathcal{D} := \lim_{n \rightarrow n_c} \mathcal{E} - \tilde{\mathcal{E}}. \quad (129)$$

In Appendix E, we show that this implies

$$\langle \mathcal{D}(0) \mathcal{D}(r) \rangle = -\frac{-2\alpha \ln(r) + \text{const.}}{r^{2x(0)}}, \quad (130)$$

$$\langle \mathcal{C}(0) \mathcal{D}(r) \rangle = \frac{\alpha}{r^{2x(0)}}, \quad (131)$$

$$\langle \mathcal{C}(0) \mathcal{C}(r) \rangle = 0, \quad (132)$$

$$\begin{aligned} \alpha &:= A(0)[x'_{\mathcal{E}}(0) - x'_{\tilde{\mathcal{E}}}(0)] \\ &\equiv \tilde{A}(0)[x'_{\mathcal{E}}(0) - x'_{\tilde{\mathcal{E}}}(0)]. \end{aligned} \quad (133)$$

These relations show that logarithms in CFTs are rather common and appear when one considers derivatives of operators with respect to a control parameter, here  $n$ . This is indeed what has been done in Eq. (119).

## VI. NUMERICAL SIMULATIONS

Let us finally verify our analytical predictions with numerical simulations.

### A. Implementation

We simulate a discretized version of the equation of motion in Eq. (1) for a string ( $d = 1$ ), using code written in Julia [86]. The lattice constant is set to 1, so that the interface position  $u_x \in \mathbb{R}$  is a vector of size  $L$ , with index  $x = \{1, \dots, L\}$ . The random forces  $F(x, u_x)$  are drawn from a Gaussian distribution with mean zero and variance one, independent for each  $x$ , and  $u_x \in \mathbb{Z}$ . For noninteger values of  $u_x$ , the force is interpolated linearly between the closest two integer neighbors. The lattice Laplacian is defined by

$$\nabla^2 u_x := u_{x-1} + u_{x+1} - 2u_x, \quad (134)$$

with  $u_0 := u_L$  and  $u_{L+1} := u_1$ . The total force acting on site  $x$  is

$$F_{\text{tot}}(u_x) := m^2(w - u_x) + \nabla^2 u_x + F(x, u_x). \quad (135)$$

The position  $u_x$  of the interface at site  $x$  is increased if the force acting on it is positive. Due to Middleton's [77] theorem, to find the pinning configurations, one can move a monomer until the force acting on it vanishes [87]. This is much more efficient than directly integrating the equation of motion in Eq. (1).

If monomer  $x$  is at position  $u \equiv u_x$ , we can estimate the total force acting on it at position  $u + \delta u$  as

$$F_{\text{tot}}(u + \delta u) = F_{\text{tot}}(u) + \frac{\partial F_{\text{tot}}(x, u)}{\partial u} \delta u. \quad (136)$$

This estimate is valid if  $u_x + \delta u$  is smaller than the next integer, and we use the right-hand derivative at integer  $u_x$ . In our

algorithm,  $\frac{\partial F_{\text{tot}}(x,u)}{\partial u} = \partial_u F(x, u) - m^2 - 2$ . If Eq. (136) is positive when evaluated at the next integer, shift  $u$  to this value. If this is not the case, we move by  $\delta u = -F_{\text{tot}}(u)/\frac{\partial F_{\text{tot}}(x,u)}{\partial u}$ , such that at the end of the move  $F_{\text{tot}}$  vanishes.

### B. Measurement of $\Delta(w)$

We measure  $\Delta(w)$  and its second cumulant (variance). To get rid of boundary effects, we need to choose the system size big enough. From FRG, we know that  $\Delta(w)$  becomes independent of  $L$  in the limit  $mL \rightarrow \infty$ . In that limit, the spatial correlation function  $\overline{[u(x) - u(y)]^2}$  decays exponentially as  $\exp(-m|x - y|)$ , which we associate with a correlation length  $\xi = \frac{1}{m}$ . This means that

$$\begin{aligned} \Delta(w, w') &:= \frac{m^4}{L^d} \int_x \int_y \overline{[u_w(x) - w][u_{w'}(y) - w']^c} \\ &= m^4 \int_y \overline{[u_w(x) - w][u_{w'}(y) - w']^c} \\ &\approx m^4 \xi^d \overline{[u_w(x) - w][u_{w'}(x) - w']^c}, \end{aligned} \quad (137)$$

where we used the spatial exponential decay with correlation length  $\xi \ll L$ . Since the disorder forces  $F(x, u)$  are statistically invariant under translations in  $u$ , Eq. (137) only depends on  $|w - w'|$ , and we write it as

$$\Delta(w - w') := \Delta(w, w'). \quad (138)$$

We see that Eq. (137) does not depend on  $L$  if  $\xi \ll L$ . As we saw in the analytic part and will later confirm in the simulations, the function  $\Delta(w)$  decays itself approximately exponentially  $\Delta(w) \approx \Delta(0) \exp(-\rho_m w)$ , which allows us to define an *effective disorder correlation length*  $\rho_m$  by (see Fig. 1)

$$\rho_m := \frac{\Delta(0)}{|\Delta'(0^+)|}. \quad (139)$$

This is close to the more natural-looking definition:

$$\rho'_m := \frac{\int_w w \Delta(w)}{\int_w \Delta(w)}. \quad (140)$$

We use the definition in Eq. (139) rather than in Eq. (140) for two reasons: First, the latter is difficult to use analytically due to the integral; second, in simulations or experiments, the tail of  $\Delta(w)$  has large statistical errors, which gives a large overall error for  $\rho'_m$ .

The variance of  $\Delta := \Delta(u)$ , which quantifies the statistical error, can (for each  $u$ ) be estimated from

$$\text{var}(\Delta) := \frac{\overline{\Delta^2} - \overline{\Delta}^2}{N}, \quad (141)$$

where  $N$  is the number of independent samples.

To use Eq. (141), we need to get rid of statistically dependent samples. This is achieved by using

$$\text{var}(\Delta) := \frac{\overline{\Delta^2} - \overline{\Delta}^2}{N_{\text{eff}}}, \quad N_{\text{eff}} \approx \frac{N}{3\rho/\delta w}, \quad (142)$$

where  $N$  is the number of samples,  $\delta w$  the step size in the simulation between samples taken for  $\Delta$ , and  $\rho_m$  the correlation

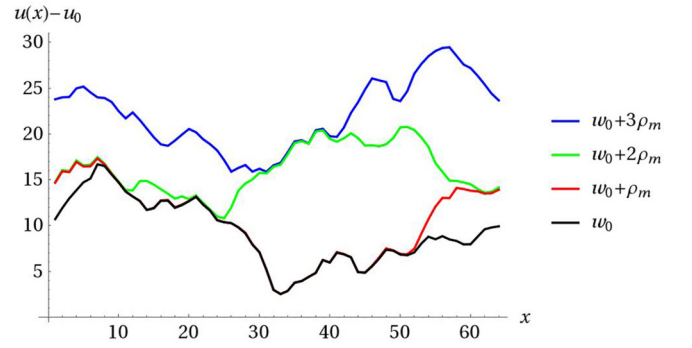


FIG. 10.  $u(x) - u_0$  for  $L = 64$ , and  $mL = 8$ . Between successive samples, the control parameter  $w$  is increased by  $\rho_m$ , starting at  $w = w_0$ . We see that augmenting  $w$  by the correlation length  $\rho_m$  (in the  $u$  direction),  $u(x)$  takes a different configuration at a substantial fraction of sites.

length defined in Eq. (139). This is a conservative estimate, assuming that a new independent sample is generated if  $w$  is advanced by  $3\rho_m$ . It can indeed be seen in the example in Fig. 10 that, when advancing  $w$  to  $w + 3\rho_m$ , the whole line has moved, which reinforces this argument.

To show explicitly in the simulations the independence of  $\Delta(w)$  on  $L$  in the limit of large  $mL$ , we need to eliminate the factors of  $m$ . By definition,  $u_w(x) - w$  scales as  $m^{-\xi}$ , and  $\Delta(w) \sim m^{4-d} u^2 \sim m^{4-d-2\xi}$ , where we used  $\xi = 1/m$  in Eq. (137). This allows us to define the dimensionless correlator  $\tilde{\Delta}(w)$ :

$$\tilde{\Delta}(w) := m^{d-4+2\xi} \Delta(wm^\xi). \quad (143)$$

Note that this definition is not unique, as one can rescale  $\tilde{\Delta}(w) \rightarrow \lambda^{-2} \tilde{\Delta}(w\lambda)$ . Before considering the results of the numerical simulations, there is a last point we need to address: Eq. (137) contains a connected average, so one should measure  $\overline{u_w(x) - w}$  first. This can be avoided, by sampling the combination:

$$\Delta(0) - \Delta(w) = \frac{1}{2} \frac{m^4}{L^d} \int_x \int_y \overline{[u_w(x) - w - u_{w'}(y) + w']^2}^c. \quad (144)$$

It is this combination we display in Figs. 11 and 12. Figure 11 shows that the limit of  $L \rightarrow \infty$  exists, at fixed  $mL$ . While a

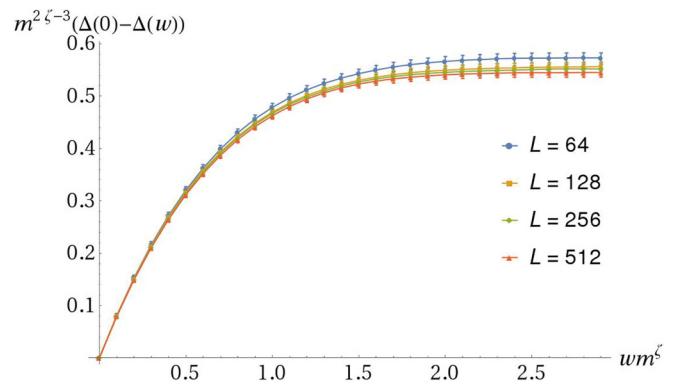


FIG. 11.  $\tilde{\Delta}(0) - \tilde{\Delta}(w)$  for  $mL = 4$ .

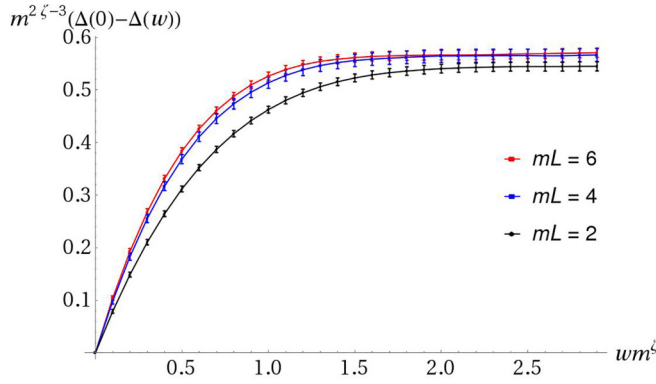


FIG. 12.  $\tilde{\Delta}(0) - \tilde{\Delta}(w)$  for  $mL = 2, 4$ , and  $6$ , in a system of size  $L = 1024$ .

system of size  $L = 64$  is certainly too small,  $L = 512$  is large enough to exhibit this limiting behavior. Figure 12 analyzes what happens when  $mL$  is taken larger, at fixed system size  $L = 1024$ . The conclusion is that one should use  $mL \geq 6$  to have negligible finite-size effects, physically caused by system-spanning avalanches.

### C. Comparison of $\Delta(w)$ to the theory

We now compare the shape of  $\Delta(w)$  obtained from simulations to results from field theory, see Fig. 14. This is delicate, as a direct  $\epsilon$  expansion is badly converging. At 2-loop order, we can use a Padé approximant:

$$\begin{aligned} \Delta(w) &= \epsilon \Delta_1(w) + \epsilon^2 \Delta_2(w) + O(\epsilon^3) \\ &= \epsilon \frac{\Delta_1(w) + \alpha \epsilon \Delta_2(w)}{1 + \epsilon(\alpha - 1) \frac{\Delta_2(w)}{\Delta_1(w)}} + O(\epsilon^3). \end{aligned} \quad (145)$$

Our strategy is to use  $\alpha$  to improve convergence; more specifically, we choose  $\alpha$ , such that, in  $d = 0$ , we recover as precisely as possible the exact solution of Ref. [88]. As can be seen in Fig. 13, this is achieved for  $\alpha = 0.35$ . Using this value of  $\alpha$ , we predict the shape of  $\Delta(w)$  in  $d = 1$ , see Fig. 13. This approach works well at two loops for which it was used in Ref. [8]. In contrast, we were not able to properly resum the  $\epsilon$  expansion for  $\Delta(w)$  at 3-loop order. Our failed attempts, using Padé resummation and rescaling invariance for optimization, are documented in Appendix F.

We finally compare our simulation result (for  $mL = 6$ ,  $L = 1024$ ) in dimension  $d = 1$  to the simulation results from Ref. [89] in  $d = 1$  ( $L = 8192$ ). As can be seen in Fig. 13, both simulations agree well. We also show simulation results in  $d = 2$ . From experiments [8] and continuity of the curves, we expect  $\Delta(w)$  in  $d = 2$  to lie between its counterparts in dimensions  $d = 1$  and  $4$ . As Fig. 13 shows, this does not seem to be the case. We expect the system size used in Ref. [89] to be too small for  $\Delta(w)$  to be in the asymptotic regime.

### D. Critical force

We finally compare predictions to simulations for the critical force, defined as

$$f_c = m^2 \overline{(w - u_w)}. \quad (146)$$

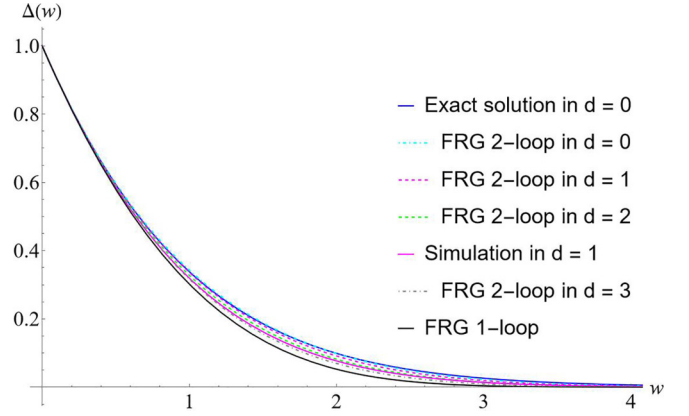


FIG. 13. Shape comparison: 1-loop functional renormalization group (FRG; black, bottom curve), exact solution in dimension  $d = 0$  (blue solid, top curve), Padé resummed 2-loop result from Eq. (145) in  $d = 0$  for  $\alpha = 0.35$  (cyan, dotted), the same Padé in  $d = 1$  (magenta, dashed), the same Padé in  $d = 2$  (green, dashed), our simulations in dimension  $d = 1$  (magenta, solid), and the same Padé in  $d = 3$  (gray, dot-dashed).

For large enough  $mL$ , it does not depend on  $L$  for the same reasons as  $\Delta(w)$ . Equation (108) predicts that

$$f_c = f_c^0 - \mathcal{B} m^2 \rho_m + O(m^2), \quad (147)$$

where  $\rho_m$  is

$$\rho_m = \frac{\Delta(0)}{|\Delta'(0^+)|} =: \hat{\rho} m^{-\zeta}. \quad (148)$$

To find  $\hat{\rho}$  (a numerical value of the simulation), we plot  $\hat{\rho} = \rho_m m^\zeta$ , which we evaluate for small  $m$ . In Fig. 15, we find that

$$\hat{\rho} = 0.531 \pm 0.05. \quad (149)$$

In Fig. 16, we then plot  $f_c m^{\zeta-2}$  against  $m^{\zeta-2}$ , which yields

$$b \equiv \mathcal{B} \hat{\rho} = 0.970 \pm 0.05. \quad (150)$$

As we see in Fig. 16, for small  $m$ , the critical force  $f_c(m)$  depends linearly on  $m^{2-\zeta}$ . From that, we deduce that the  $O(m^2)$  in Eq. (107) is seemingly very small or absent. Together with the results for  $\hat{\rho}$  shown in Fig. 16, this gives our final result

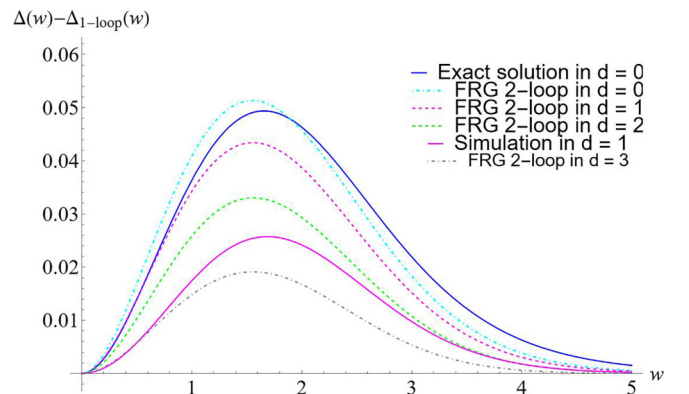


FIG. 14. Shape comparison of  $\Delta(w) - \Delta_{1\text{-loop}}(w)$ , with colors as in Fig. 13.



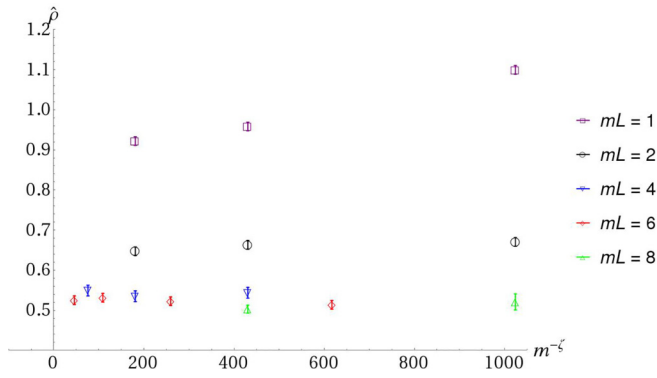


FIG. 15.  $\hat{\rho}$  as a function of  $m^{-\zeta}$ , for different  $mL$ , and different system sizes. The larger systems are to the right.

for  $\mathcal{B}$  as

$$\mathcal{B} = 1.8 \pm 0.2. \quad (151)$$

This is in reasonable agreement with the values reported in Sec. IV D. Note that  $\mathcal{B}$  does not depend on the elastic coefficient  $c$ . This is demonstrated in Appendix G.

## VII. CONCLUSIONS

In this paper, we calculated the roughness exponent  $\zeta$  to 3-loop order. Using analytic information in dimension  $d = 0$  and Borel resummation allows us to give excellent values for the roughness  $\zeta$  in all dimensions, including  $d = 1$ . The predictive power for the shape of the renormalized disorder correlator is weaker: We estimate it to be good in dimension  $d = 3$ , satisfactory in  $d = 2$ , but insufficient in dimension  $d = 1$ . It is not clear how to implement a Borel resummation for a whole function.

We further considered the critical force at depinning and showed that it has a universal amplitude predicted by the field theory. Our numerical simulations in dimension  $d = 1$  confirm this prediction. This may prove useful in analyzing finite-size corrections in experiments.

We finally considered CDWs, which are related to loop-erased random walks and the  $O(n)$  model at  $n = -2$ .

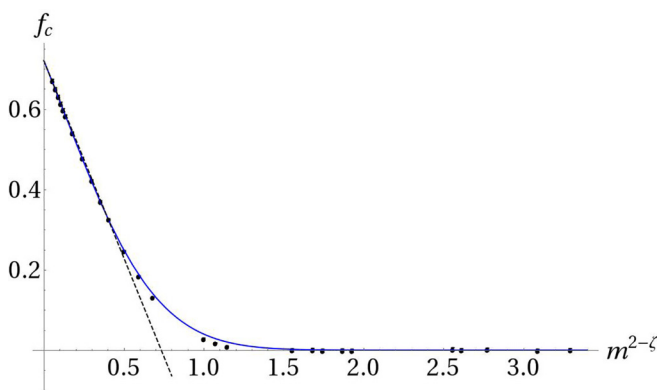


FIG. 16.  $f_c$  as a function of  $m^{-\zeta}$  for  $mL = 4$ . The fit used to extrapolate to  $m = 0$  is via an exponential function  $f_c = f_c^0 \exp(-bm^{-\zeta})$ , with the two fit parameters  $f_c^0$  and  $b$ . The slope indicated with a dashed line is  $-b \equiv \mathcal{B}\hat{\rho}$ , as given in Eq. (150).

We find that the amplitude of the critical force at depinning has a logarithmic dependence on the regularization scale and that this can be understood in the framework of log-CFT.

It would be interesting to also obtain the corrections to the dynamical exponent  $z$ , and we made some progress in this direction. The diagrams which need to be evaluated are much more involved, as sums of squared independent loop momenta appear in the denominator [see Eq. (30)], and the number of independent diagrams may well be a hundred. For this reason, we decided to postpone their analysis to the future.

With the 3-loop result at hand, another open question can be tackled, namely, the large-order behavior of functional field theories, i.e., theories where the coupling constant is not a number but a function. We hope to report progress in this direction soon.

## ACKNOWLEDGMENT

We thank Andrei Fedorenko, Jesper Jacobsen, Gauthier Mukherjee, and Alberto Rosso for discussions.

## APPENDIX A: LOOP INTEGRALS

Here, we give all loop integrals necessary for the main text. Some of them are calculated directly, while the remaining ones can be found in Ref. [66].

### 1. The integral $I_1$

The integral  $I_1$  is defined as

$$I_1 = \text{loop diagram} := \int_k \frac{1}{(k^2 + m^2)^2}. \quad (A1)$$

It is calculated as follows:

$$\begin{aligned} I_1 &= \int_k \int_0^\infty d\alpha \alpha \exp(-\alpha(k^2 + m^2)) \\ &= \left( \int_k \exp(-k^2) \right) \int_0^\infty d\alpha \alpha^{1-(d/2)} \exp(-\alpha m^2) \\ &= \left( \int_k \exp(-k^2) \right) m^{-\epsilon} \Gamma\left(\frac{\epsilon}{2}\right). \end{aligned} \quad (A2)$$

This gives us the normalization constant for higher-loop calculations:

$$(\epsilon I_1) = m^{-\epsilon} \left[ \int_k \exp(-k^2) \right] \epsilon \Gamma\left(\frac{\epsilon}{2}\right). \quad (A3)$$

### 2. The tadpole diagram $I_{\text{tp}}$

Using that

$$-\frac{\partial}{\partial(m^2)} \text{tadpole diagram} = \text{loop diagram} \quad (A4)$$

we get by integration that

$$\text{tadpole diagram} = \frac{2m^2}{(d-4)(d-2)} (\epsilon I_1). \quad (A5)$$

### 3. The integral $I_A$

$$\begin{aligned}
 I_A &= \text{Diagram: Triangle with a double line on the bottom edge.} \\
 &= \left[ \frac{1}{2\epsilon^2} + \frac{1}{4\epsilon} + \frac{27+3\psi'(\frac{5}{6})-3\psi'(\frac{1}{3})-4\pi^2}{216} + O(\epsilon) \right] (\epsilon I_1)^2 \\
 &= \left[ \frac{1}{2\epsilon^2} + \frac{1}{4\epsilon} + \frac{1-4C_3}{8} + O(\epsilon) \right] (\epsilon I_1)^2
 \end{aligned} \tag{A6}$$

In the first line, we gave the raw result obtained via computer algebra [66]. The reflection properties of the  $\Gamma$  function combined with the duplication and triplication formulas [90] give nontrivial relations, which following Refs. [66,67] are used to combine all nontrivial terms into a single number  $C_3$ :

$$\psi'\left(\frac{5}{6}\right) - \psi'\left(\frac{1}{3}\right) = 4\pi^2 - 5\psi'\left(\frac{1}{3}\right) + \psi'\left(\frac{2}{3}\right), \tag{A7}$$

$$\psi'\left(\frac{1}{3}\right) + \psi'\left(\frac{2}{3}\right) = \frac{4\pi^2}{3}, \tag{A8}$$

$$\psi'\left(\frac{1}{6}\right) + \psi'\left(\frac{5}{6}\right) = 4\pi^2, \tag{A9}$$

$$C_3 = \frac{\psi'\left(\frac{1}{3}\right)}{6} - \frac{\pi^2}{9} \approx 0.585977. \tag{A10}$$

### 4. The sunset diagram

$$I_{ss} = \text{Diagram: Two vertices connected by two parallel lines.} \tag{A11}$$

This diagram can be reduced to  $I_A$  given in Eq. (A6):

$$-\frac{\partial}{\partial(m^2)} \text{Diagram: Two vertices connected by two parallel lines with a double line on the top edge.} = 3 \text{Diagram: Triangle with a double line on the bottom edge.} \tag{A12}$$

Using Eq. (A6), this implies

$$I_{ss} = m^2 \left[ -\frac{3}{2\epsilon^2} - \frac{9}{4\epsilon} - \frac{3(7-4C_3)}{8} + \dots \right] (\epsilon I_1)^2. \tag{A13}$$

### 5. The integral $I_m \equiv I_o$

$$\begin{aligned}
 I_m &= \text{Diagram: Two vertices connected by two parallel lines, each with a double line.} \equiv I_o = \text{Diagram: Two vertices connected by two parallel lines, each with a double line and a double line on the bottom edge.} \\
 &= \left[ \frac{1}{3\epsilon^3} + \frac{1}{3\epsilon^2} + \frac{1-6C_3}{6\epsilon} + O(\epsilon) \right] (\epsilon I_1)^3.
 \end{aligned} \tag{A14}$$

### 6. The star integral $I_i$

$$\begin{aligned}
 I_i &= \text{Diagram: Three vertices in a triangle, each connected to the other two by a double line.} \\
 &= \frac{\zeta(3)}{2\epsilon} (\epsilon I_1)^3 + O(\epsilon^0) \\
 &= \frac{0.601028}{\epsilon} (\epsilon I_1)^3 + O(\epsilon^0).
 \end{aligned} \tag{A15}$$

### 7. The integral $I_j$

$$I_j = \text{Diagram: Square with a diagonal line and a double line on the diagonal.} = \left[ \frac{1}{3\epsilon^3} + \frac{1}{6\epsilon^2} + \frac{1}{12\epsilon} + \dots \right] (\epsilon I_1)^3. \tag{A16}$$

### 8. The integral $I_l$

$$\begin{aligned}
 I_l &= \text{Diagram: Square with a diagonal line and a double line on the top edge.} \\
 &= \left[ \frac{1}{6\epsilon^3} + \frac{1}{4\epsilon^2} + \frac{7-12C_3}{24\epsilon} + O(\epsilon) \right] (\epsilon I_1)^3.
 \end{aligned} \tag{A17}$$

### 9. The integral $I_r$

$$I_r = \text{Diagram: Triangle with a double line on the bottom edge and a double line on the top edge.} \tag{A18}$$

This integral can be reduced to known integrals via a derivative with respect to  $m^2$ :

$$\begin{aligned}
 -\frac{\partial}{\partial(m^2)} \text{Diagram: Triangle with a double line on the bottom edge.} &= \text{Diagram: Square with a diagonal line and a double line on the diagonal.} + 4 \text{Diagram: Square with a diagonal line and a double line on the top edge.} \\
 &= \left[ \frac{1}{\epsilon^3} + \frac{4}{3\epsilon^2} + \frac{\frac{4}{3} - 3C_3}{\epsilon} + O(\epsilon^0) \right] (\epsilon I_1)^3.
 \end{aligned} \tag{A19}$$

Integrating yields

$$\begin{aligned}
 I_r &= \text{Diagram: Triangle with a double line on the bottom edge and a double line on the top edge.} \\
 &= m^2 (\epsilon I_1)^3 \left[ -\frac{1}{\epsilon^3} - \frac{17}{6\epsilon^2} + \frac{36C_3 - 67}{12\epsilon} + O(\epsilon^0) \right].
 \end{aligned} \tag{A20}$$

### 10. The integral $I_1$ for a finite system

Define

$$\begin{aligned}
 I_1^{\text{discrete}}(m, L, d) &:= \frac{1}{L^d} \sum_{\vec{n}} \frac{1}{\left[ \left( \frac{2\pi\vec{n}}{L} \right)^2 + m^2 \right]^2} \\
 &= \frac{1}{m^4 L^d} \sum_{\vec{n}} \frac{1}{\left[ \left( \frac{2\pi\vec{n}}{mL} \right)^2 + 1 \right]^2}.
 \end{aligned} \tag{A21}$$

If  $mL \gg 1$ , this can be approximated by an integral  $\sum_{\vec{n}} \rightarrow \int d^d \vec{n}$ :

$$\begin{aligned}
 I_1^{\text{discrete}}(m, L, d) &= \frac{(mL)^d}{m^4 L^d} \int \frac{d^d \vec{n}}{(2\pi)^d (\vec{n}^2 + 1)^2} \\
 &= m^{-\epsilon} \int \frac{d^d \vec{n}}{(2\pi)^d (\vec{n}^2 + 1)^2}.
 \end{aligned} \tag{A22}$$

This integral is given in Eq. (A2). On the other hand,

$$\begin{aligned}
I_1^{\text{discrete}}(m, L, d) &= L^{4-d} \sum_{\vec{n}} \frac{1}{[(2\pi\vec{n})^2 + (mL)^2]^2} \\
&= L^{4-d} \int_{s>0} s \left[ \sum_{n=-\infty}^{\infty} \exp(-s(2\pi n)^2) \right] \exp(-s(mL)^2) \\
&= L^{4-d} \int_{s>0} s \vartheta_3(0, \exp(-4\pi^2 s))^d \exp(-s(mL)^2).
\end{aligned} \tag{A23}$$

Therefore,

$$\begin{aligned}
\mathcal{I}_1(mL, d) &:= m^4 L^d I_1^{\text{discrete}}(m, L, d) \\
&= (mL)^4 \int_{s>0} s \vartheta_3(0, \exp(-4\pi^2 s))^d \\
&\quad \times \exp(-s(mL)^2) \\
&= \int_{s>0} s \vartheta_3\left(0, \exp\left(-\frac{4\pi^2 s}{(mL)^2}\right)\right)^d \exp(-s).
\end{aligned} \tag{A24}$$

For small  $mL$ , one has

$$\lim_{x \rightarrow 0} \mathcal{I}_1(x, d) = 1. \tag{A25}$$

In the limit of large  $mL$ , this gives

$$\mathcal{I}_1(mL, d) \simeq \frac{1}{(4\pi)^{d/2}} \Gamma\left(\frac{4-d}{2}\right) (mL)^d, \tag{A26}$$

$$\frac{\Gamma\left(\frac{4-d}{2}\right)}{(4\pi)^{d/2}} = \begin{cases} \frac{1}{4} & \text{in } d = 1 \\ \frac{1}{4\pi} & \text{in } d = 2 \\ \frac{1}{8\pi} & \text{in } d = 3. \end{cases} \tag{A27}$$

## APPENDIX B: DETAILS FOR CDWs

### 1. $f_c$ for CDWs in the limit of $d \rightarrow 2$

In  $d = 2$ , we have

$$v = \frac{1}{2 - 2h_{1,3}} = \frac{1}{4} \left[ 1 + \frac{\pi}{\arccos\left(\frac{\eta}{2}\right)} \right], \tag{B1}$$

$$\begin{aligned}
\eta &= 4h_{(1/2),0} \\
&= \frac{5}{4} - \frac{3 \arccos\left(\frac{\eta}{2}\right)}{4\pi} - \frac{\pi}{\arccos\left(\frac{\eta}{2}\right) + \pi}.
\end{aligned} \tag{B2}$$

Sadly,

$$-\partial_n \left[ \frac{1}{v} + \eta \right]_{d=2} \sim \frac{1}{\sqrt{n+2}}. \tag{B3}$$

This may be related to the naturally appearing explicit factor of  $1/(2 - \epsilon)$ . The latter comes when relating diagrams for  $f_c$  to derivatives of known diagrams correcting the disorder. Undoing this integration then leads to a factor of  $1/(2 - \epsilon) = 1/(d - 2)$ , see, e.g., Eq. (A5).

### 2. The critical force as an observable inside the theory at $n = -2$

We find that Eq. (119) can be calculated as follows in the theory at  $n = -2$ :

$$-\frac{g}{2} \left\langle \phi_2(x) \phi_1(x)^2 \exp\left(-\frac{g}{8} \int (\vec{\phi}^2)^2\right) \right\rangle_{0|_{n=-2}} = f_c \phi_2. \tag{B4}$$

In principle, one should retain only 1PI diagrams, but this does not seem to be necessary. The reason is probably that disconnected and 1PR diagrams have additional factors of  $(n+2)$ . The idea behind this contraction is to apply  $\partial_n \phi^2$  to the interaction, which leads to something like  $\phi_1^2(\vec{\phi}^2)$ . The additional component is represented by  $\phi_1^2$ ; the problem is that it should not be equal to the other fields in the interaction. Thus, the idea is to start constructing  $\Gamma^{(2)}$  by selecting one external leg with component number 2 and then restricting the multiplying factor of  $\vec{\phi}^2$  to a distinct component. The reason for pulling out only one external (uncontracted) field is that, otherwise, we could either derive the same vertex twice or two vertices once each, which would complicate the writing.

An alternative formula is

$$\begin{aligned}
&-\frac{g}{8} \left[ \phi_1(x) - \phi_2(x) \right] \left[ \phi_1(x)^2 + \phi_2(x)^2 \right] \\
&\quad \times \exp\left(-\frac{g}{8} \int (\vec{\phi}^2)^2\right) \Big|_{0|_{n=-2}} = f_c (\phi_1 - \phi_2),
\end{aligned} \tag{B5}$$

i.e., we drop the space dependence as usual. Another alternative is

$$-\frac{g}{6} \sum_i \phi_i(x)^3 e^{-S} \rightarrow f_c \sum_i \phi_i. \tag{B6}$$

Still another alternative is

$$-\frac{g}{6} \phi_1(x)^3 e^{-S} \rightarrow f_c \phi_1. \tag{B7}$$

This is given in the main text.

### 3. The critical force with complex fields

This can also be done with  $N$  complex fields in the limit of  $N \rightarrow -1$ . We use the action:

$$\begin{aligned}
\mathcal{S} &= \int_x \nabla \vec{\phi}^*(x) \nabla \vec{\phi}(x) + m^2 \vec{\phi}^*(x) \vec{\phi}(x) \\
&\quad + \frac{g}{2} [\vec{\phi}^*(x) \vec{\phi}(x)]^2.
\end{aligned} \tag{B8}$$

We find up to 4-loop order

$$-\frac{g}{2} \phi_1^*(x) \phi_2^*(x) \phi_2(x) e^{-S} \Big|_{N=-1} \rightarrow f_c \phi_1^*. \tag{B9}$$

Another option is (gain checked up to 4-loop order):

$$-\frac{g}{4} \phi_1^*(x) \phi_1^*(x) \phi_1(x) e^{-S} \Big|_{N=-1} = f_c \phi_1^*. \tag{B10}$$

The rationale connecting these two observables is that

$$\begin{aligned}
&-\frac{g}{2} \phi_1^*(x) \sum_i \phi_i^*(x) \phi_i(x) e^{-S} \\
&= -\frac{g}{2} \phi_1^*(x) \phi_1^*(x) \phi_1(x) e^{-S}
\end{aligned}$$

$$\begin{aligned}
 & -\frac{g}{2}(N-1)\phi_1^*(x)\phi_2^*(x)\phi_2(x)e^{-S} \\
 & \rightarrow f_c\phi_1^*[2+(N-1)] \rightarrow 0 \quad \text{at } N = -1. \quad (\text{B11})
 \end{aligned}$$

### APPENDIX C: UV-CUTOFF-DEPENDENT CONTRIBUTIONS TO THE CRITICAL FORCE

In the preceding sections, all diagrams were calculated within dimensional regularization, i.e., without an explicit short-distance, i.e. ultraviolet (UV) cutoff. However, this is incorrect, as all diagrams have a strong UV divergence. Here, we wish to show that these additional UV-cutoff-dependent terms are either independent of  $m$ , or at least this dependence vanishes when we take  $\Lambda$  large.

There are two relatively simple ways to put an UV cutoff:

$$I_{\text{tp}}^{\text{hard}} := \text{Diagram} = \int_k \frac{1}{k^2 + m^2} \Theta(|k| \leq \Lambda), \quad (\text{C1})$$

$$I_{\text{tp}}^{\text{soft}} := \text{Diagram} = \int_k \frac{1}{k^2 + m^2} e^{-ak^2}, \quad (\text{C2})$$

$$a = \frac{1}{\Lambda^2}, \quad (\text{C3})$$

where  $\Lambda$  is a UV scale, of the same engineering dimension as  $m$ . The soft cutoff gives

$$\begin{aligned}
 \frac{I_{\text{tp}}^{\text{soft}}}{\epsilon I_1|_{m=1}} &= -\frac{(2 - \frac{d}{2})\Lambda^{d-2} \exp(am^2) E_{d/2}(\frac{m^2}{\Lambda^2})}{(d-4)\Gamma(3 - \frac{d}{2})} \\
 &= \frac{\Lambda^{d-2}}{(d-2)\Gamma(3 - \frac{d}{2})} + \frac{2m^{d-2}}{(d-4)(d-2)} + O(\Lambda^{-1}), \quad (\text{C4})
 \end{aligned}$$

where  $E$  is the ExpIntegralE function.

The hard cutoff gives

$$\begin{aligned}
 \frac{I_{\text{tp}}^{\text{hard}}}{\epsilon I_1|_{m=1}} &= -\frac{4\Lambda^d \sin(\frac{\pi d}{2}) {}_2F_1(1, \frac{d}{2}; \frac{d+2}{2}; -\frac{\Lambda^2}{m^2})}{\pi(4-d)(d-2)dm^2} \\
 &= \frac{4\Lambda^{d-2} \sin(\frac{\pi d}{2})}{\pi(d-4)(d-2)^2} + \frac{2m^{d-2}}{(d-4)(d-2)} + \dots \quad (\text{C5})
 \end{aligned}$$

The strong UV divergence can be extracted by applying a  $\Lambda$  derivative:

$$\begin{aligned}
 \Lambda \partial_\Lambda \frac{I_{\text{tp}}^{\text{hard}}}{\epsilon I_1|_{m=1}} &= \frac{4 \sin(\frac{\pi d}{2})}{\pi(d-4)(d-2)} \frac{\Lambda^d}{m^2 + \Lambda^2} \\
 &\sim \Lambda^{d-2} + O(m^2)\Lambda^{d-4}. \quad (\text{C6})
 \end{aligned}$$

The first term is  $m$  independent; the second disappears in dimension  $d < 4$  for  $\Lambda \rightarrow \infty$ .

Let us now apply this to the 2-loop sunset integral:

$$\Lambda \partial_\Lambda I_{\text{ss}} \sim \frac{3\Lambda^d}{m^2 + \Lambda^2} \int_k \frac{\Theta(|k| \leq \Lambda) \Theta(|k + \Lambda| \leq \Lambda)}{(k^2 + m^2)[(k + \Lambda)^2 + m^2]}. \quad (\text{C7})$$

The last factor has no long-distance, i.e. infrared (IR) singularity at  $k \rightarrow 0$  or  $k \rightarrow \Lambda$ . It can globally be bounded by  $\Lambda^{d-4}$ ; for  $k \rightarrow 0$ , it goes as  $m^{d-2}\Lambda^{-2}$ . All these terms are IR finite in the limit of  $\Lambda \rightarrow \infty, m \rightarrow 0$ .

For the 3-loop integral, in a hard-cutoff scheme:

$$\Lambda \partial_\Lambda \text{Diagram} = \text{Diagram} + 4 \text{Diagram}, \quad (\text{C8})$$

where the open circle indicates the momentum vector put to  $\Lambda$ . For the first, the momentum  $\Lambda$  traverses both loops, such that

$$\text{Diagram} = \text{IR-finite}. \quad (\text{C9})$$

Only the last diagram can give a contribution:

$$\text{Diagram} \simeq \Lambda^{-\epsilon} \times \frac{m^{-\epsilon}}{\epsilon} \times m^{d-2}. \quad (\text{C10})$$

We expect the factor of  $m^{-\epsilon}/\epsilon$  coming from the subdivergence in the lower loop to be canceled by a counterterm of the disorder.

### APPENDIX D: CRITICAL FORCE IN $d = 0$

In  $d = 0$ , according to Ref. [91]:

$$\begin{aligned}
 f_c &\simeq \sqrt{2 \ln(m^{-2})} + \frac{\gamma_E}{\sqrt{2 \ln(m^{-2})}} \\
 &+ \dots, \quad \text{Eq. (70) of Ref. [91],}
 \end{aligned}$$

$$\rho_m \simeq \frac{1}{m^2 \sqrt{2 \ln(m^{-2})}}, \quad \text{Eq. (58) of Ref. [91],}$$

$$\Delta(w) = m^4 \rho_m^2 \tilde{\Delta}\left(\frac{w}{\rho_m}\right), \quad \text{Eq. (60) of Ref. [91].} \quad (\text{D1})$$

This gives in  $d = 0$  the two combinations of the main text:

$$\tilde{\Delta} m^2 \rho_m = \frac{\tilde{\Delta}}{\sqrt{2 \ln(m^{-2})}}, \quad (\text{D2})$$

$$|f_c| = \sqrt{2 \ln(m^{-2})} + \frac{\gamma_E}{\sqrt{2 \ln(m^{-2})}} + \dots \quad (\text{D3})$$

To our disappointment, the singularities of these two terms are different, so that we cannot obtain the amplitude  $\tilde{\Delta}$  in  $d = 0$ .

### APPENDIX E: A WORKED-OUT EXAMPLE: LOGARITHMIC OPERATORS FOR SELF-AVOIDING POLYMERS

Following Cardy [70], (see Ref. [69] for an extended review), we consider the logarithms appearing for self-avoiding polymers. To this aim, we introduce the polymer density in the  $\phi^4$  field theory for polymers [92], which transforms as a singlet under  $O(n)$  [93]:

$$\mathcal{E}_i := \phi_i^2, \quad \mathcal{E} := \frac{1}{n} \sum_{i=1}^n \phi_i^2. \quad (\text{E1})$$

Next, we consider the traceless vector:

$$\tilde{\mathcal{E}}_i := \phi_i^2 - \frac{1}{n} \sum_{j=1}^n \phi_j^2 \equiv \mathcal{E}_i - \mathcal{E}. \quad (\text{E2})$$

Alternatively, one can use the traceless tensor operator, which sits in the same multiplet:

$$\tilde{\mathcal{E}}_{ij} := \phi_i \phi_j - \frac{1}{n} \delta_{ij} \sum_{k=1}^n \phi_k^2. \quad (\text{E3})$$

In these notations,

$$x_{\mathcal{E}}(n) = \dim_{\mu}(\mathcal{E}) = d - y_{\mathcal{E}} = d - 2 - \gamma_{\phi^2} + \eta, \quad (\text{E4})$$

$$x_{\tilde{\mathcal{E}}}(n) = \dim_{\mu}(\tilde{\mathcal{E}}) = d - y_{\tilde{\mathcal{E}}} = d - 2 - \gamma_{\phi\phi} + \eta. \quad (\text{E5})$$

Then

$$\begin{aligned} \langle \mathcal{E}(r) \mathcal{E}(0) \rangle &= \frac{1}{n} [\langle \mathcal{E}_1(r) \mathcal{E}_1(0) \rangle + (n-1) \langle \mathcal{E}_1(r) \mathcal{E}_2(0) \rangle] \\ &\simeq \frac{A(n)}{n} r^{-2x_{\mathcal{E}}(n)}, \end{aligned} \quad (\text{E6})$$

$$\begin{aligned} \langle \tilde{\mathcal{E}}_i(r) \tilde{\mathcal{E}}_i(0) \rangle &= \frac{n-1}{n} [\langle \mathcal{E}_1(r) \mathcal{E}_1(0) \rangle - \langle \mathcal{E}_1(r) \mathcal{E}_2(0) \rangle] \\ &\simeq \frac{n-1}{n} \tilde{A}(n) r^{-2x_{\tilde{\mathcal{E}}}(n)}. \end{aligned} \quad (\text{E7})$$

Since the expressions in the square brackets become identical in the limit of  $n \rightarrow 0$ :

$$A(0) = \tilde{A}(0), \quad x_{\mathcal{E}}(0) = x_{\tilde{\mathcal{E}}}(0). \quad (\text{E8})$$

Consider

$$\langle \mathcal{E}(r) \mathcal{E}(0) \rangle + \langle \tilde{\mathcal{E}}_i(r) \tilde{\mathcal{E}}_i(0) \rangle = \langle \mathcal{E}_1(r) \mathcal{E}_1(0) \rangle, \quad (\text{E9})$$

$$\langle \mathcal{E}(r) \mathcal{E}(0) \rangle - \frac{1}{n-1} \langle \tilde{\mathcal{E}}_i(r) \tilde{\mathcal{E}}_i(0) \rangle = \langle \mathcal{E}_1(r) \mathcal{E}_2(0) \rangle. \quad (\text{E10})$$

This implies that

$$\begin{aligned} \langle \mathcal{E}_1(r) \mathcal{E}_2(0) \rangle &= \frac{1}{n} [A(n) r^{-2x_{\mathcal{E}}(n)} - \tilde{A}(n) r^{-2x_{\tilde{\mathcal{E}}}(n)}] \\ &= A(n) r^{-2x_{\mathcal{E}}(n)} \frac{1}{n} \left\{ 1 - \frac{\tilde{A}(n)}{A(n)} r^{2[x_{\mathcal{E}}(n) - x_{\tilde{\mathcal{E}}}(n)]} \right\} \\ &= A(0) r^{-2x_{\mathcal{E}}(0)} \left\{ \frac{A'(0) - \tilde{A}'(0)}{A(0)} + 2 \ln(r) [x'_{\tilde{\mathcal{E}}}(0) - x'_{\mathcal{E}}(0)] \right\} + O(n), \end{aligned} \quad (\text{E11})$$

$$\langle \mathcal{E}_1(r) \mathcal{E}_1(0) \rangle - \langle \mathcal{E}_1(r) \mathcal{E}_2(0) \rangle = \frac{n}{n-1} \langle \tilde{\mathcal{E}}_i(r) \tilde{\mathcal{E}}_i(0) \rangle = r^{-2x_{\tilde{\mathcal{E}}}(n)} \tilde{A}(n), \quad (\text{E12})$$

$$\langle \mathcal{E}_1(r) \mathcal{E}_1(0) \rangle = A(0) r^{-2x_{\mathcal{E}}(0)} \left\{ 1 + \frac{A'(0) - \tilde{A}'(0)}{A(0)} + 2 \ln(r) [x'_{\tilde{\mathcal{E}}}(0) - x'_{\mathcal{E}}(0)] \right\} + O(n). \quad (\text{E13})$$

As a consequence, the ratio reads

$$\begin{aligned} \frac{\langle \mathcal{E}_1(r) \mathcal{E}_2(0) \rangle}{\langle \mathcal{E}_1(r) \mathcal{E}_1(0) \rangle - \langle \mathcal{E}_1(r) \mathcal{E}_2(0) \rangle} &= \frac{A'(0) - \tilde{A}'(0)}{A(0)} + 2 \ln(r) [x'_{\tilde{\mathcal{E}}}(0) - x'_{\mathcal{E}}(0)] + O(n). \end{aligned} \quad (\text{E14})$$

Denoting a self-avoiding polymer by a colored circle, the left-hand side can be written as

$$\frac{\langle \mathcal{E}_1(x) \mathcal{E}_2(y) \rangle}{\langle \mathcal{E}_1(x) \mathcal{E}_1(y) \rangle - \langle \mathcal{E}_1(x) \mathcal{E}_2(y) \rangle} = \frac{1}{2} \frac{\text{Diagram 1}}{\text{Diagram 2}}. \quad (\text{E15})$$

The numerator is the probability that two ring polymers attached at  $x$  and  $y$  do not intersect. The denominator is the probability that the ends of two polymers attached at  $x$  and  $y$  are at a distance  $x - y$ . According to Eq. (E13), this ratio contains a logarithmic contribution, with a universal amplitude given by the derivatives of the critical exponents. Explicit numerical values are given in Ref. [84].

Let us finally introduce the logarithmic pair. Following Cardy [69], we define in the limit of  $n \rightarrow 0$

$$\begin{aligned} \mathcal{C} &:= \lim_{n \rightarrow 0} [x_{\mathcal{E}}(n) - x_{\tilde{\mathcal{E}}}(n)] \mathcal{E} \\ &\equiv \lim_{n \rightarrow 0} [x_{\mathcal{E}}(n) - x_{\tilde{\mathcal{E}}}(n)] \tilde{\mathcal{E}}, \end{aligned} \quad (\text{E16})$$

$$\mathcal{D} := \lim_{n \rightarrow 0} \mathcal{E} - \tilde{\mathcal{E}}. \quad (\text{E17})$$

This implies

$$\begin{aligned} \langle \mathcal{D}(0) \mathcal{D}(r) \rangle &= \lim_{n \rightarrow 0} \frac{1}{n} [A(n) r^{-2x_{\mathcal{E}}(n)} - \tilde{A}(n) r^{-2x_{\tilde{\mathcal{E}}}(n)}] \\ &= -\frac{-2\alpha \ln(r) + \text{const.}}{r^{2x(0)}}, \end{aligned} \quad (\text{E18})$$

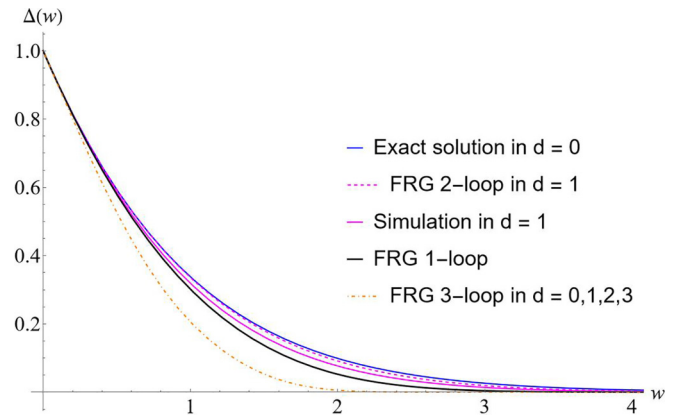


FIG. 17. Shape comparison of 1-loop functional renormalization group (FRG) result (black, thick, solid), improved 2-loop FRG result as given by Eq. (145) (magenta dashed), simulation in dimension  $d = 1$  (magenta), exact solution in dimension  $d = 0$  (blue), and 3-loop improved FRG results as given by Eq. (F1) for values of dimension  $d = 0, 1, \dots, 3$ . The last four curves (orange, dot-dashed) are indistinguishable.

TABLE III. Simulations results for  $\hat{\rho} := \rho_m m^\zeta$  (Sec. VID) and  $f_c$  for different values of  $c$ ,  $L = 128$ , and  $mL/\sqrt{c} = 4$ .

$c$	0.5	1	2	4
$f_c$	$1.14 \pm 0.05$	$0.97 \pm 0.05$	$0.87 \pm 0.05$	$0.78 \pm 0.05$
$\hat{\rho}$	$0.57 \pm 0.05$	$0.54 \pm 0.05$	$0.44 \pm 0.05$	$0.42 \pm 0.05$
$\mathcal{B}$	$2 \pm 0.2$	$1.8 \pm 0.2$	$1.98 \pm 0.2$	$1.86 \pm 0.2$

$$\begin{aligned} \langle \mathcal{C}(0)\mathcal{D}(r) \rangle &= \lim_{n \rightarrow 0} [x_{\mathcal{E}}(n) - x_{\tilde{\mathcal{E}}}(n)] \langle \mathcal{E}(0) [\mathcal{E}(r) - \tilde{\mathcal{E}}(r)] \rangle \\ &= \frac{\alpha}{r^{2x(0)}}, \end{aligned} \quad (\text{E19})$$

$$\langle \mathcal{C}(0)\mathcal{C}(r) \rangle = \lim_{n \rightarrow 0} [x_{\mathcal{E}}(n) - x_{\tilde{\mathcal{E}}}(n)]^2 \langle \mathcal{E}(0)\mathcal{E}(r) \rangle = 0. \quad (\text{E20})$$

$$\alpha = A(0)[x'_{\mathcal{E}}(0) - x'_{\tilde{\mathcal{E}}}(0)] \equiv \tilde{A}(0)[x'_{\mathcal{E}}(0) - x'_{\tilde{\mathcal{E}}}(0)]. \quad (\text{E21})$$

Here,  $(\mathcal{C}, \mathcal{D})$  forms a logarithmic pair. Denoting the dilation operator by  $\mathbb{D}$ , away from the point of degeneracy  $n = 0$ :

$$\mathbb{D} \circ \mathcal{E} = x_{\mathcal{E}}(n) \mathcal{E}, \quad (\text{E22})$$

$$\mathbb{D} \circ \tilde{\mathcal{E}} = x_{\tilde{\mathcal{E}}}(n) \tilde{\mathcal{E}}. \quad (\text{E23})$$

This implies, with  $x := x_{\mathcal{E}}(0) \equiv x_{\tilde{\mathcal{E}}}(0)$ ,

$$\mathbb{D} \circ \mathcal{C} = x \mathcal{C}, \quad (\text{E24})$$

$$\begin{aligned} \mathbb{D} \circ \mathcal{D} &= \lim_{n \rightarrow 0} x_{\mathcal{E}}(n) \mathcal{E} - x_{\tilde{\mathcal{E}}}(n) \tilde{\mathcal{E}} \\ &= \lim_{n \rightarrow 0} [x_{\mathcal{E}}(n) - x_{\tilde{\mathcal{E}}}(n)] \mathcal{E} + x_{\tilde{\mathcal{E}}}(n) [\mathcal{E} - \tilde{\mathcal{E}}] \\ &= \mathcal{C} + x \mathcal{D}. \end{aligned} \quad (\text{E25})$$

Written in matrix form, the dilatation operator has a (nondiagonalizable) block-Jordan form:

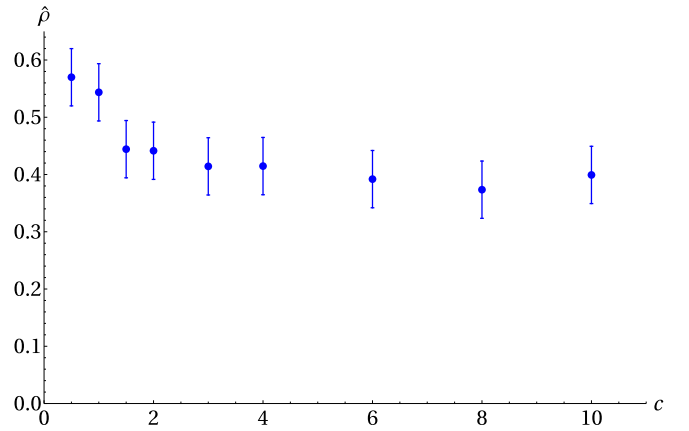
$$\mathbb{D} \circ \begin{pmatrix} \mathcal{C} \\ \mathcal{D} \end{pmatrix} = \begin{pmatrix} x & 0 \\ 1 & x \end{pmatrix} \begin{pmatrix} \mathcal{C} \\ \mathcal{D} \end{pmatrix}. \quad (\text{E26})$$

#### APPENDIX F: IMPROVEMENT OF 3-LOOP RESULT

There are two improvements we tried in our comparison between theory and simulations: The first is a Padé-resummation, as in Eq. (145), continued to 3-loop order. This strategy failed.

Our second attempt at improvement consisted of replacing

$$\begin{aligned} \Delta(w) &\rightarrow \lambda^{-2} \Delta(w\lambda), \\ \lambda &= 1 + \alpha\epsilon + \beta\epsilon^2 + O(\epsilon^3). \end{aligned} \quad (\text{F1})$$


 FIG. 18. Dependence of  $\hat{\rho}$  on  $c$ .

This transformation is an exact property of the RG equation. We then Taylor-expand Eq. (F1) to order  $\epsilon^3$  and drop the higher-order terms. Let us stress that there is no natural choice for  $\lambda$  or choice of setting  $\Delta(0) \stackrel{\dagger}{=} \epsilon/3$ , which forces higher-order corrections to vanish at  $w = 0$ . It is one particular choice, maybe not the best. This procedure helps us enforce some physical properties of  $\Delta(w)$ , the most important one being that it has its maximum at  $w = 0$  and then decays linearly for small  $w$ . We succeeded to achieve this, but we were unable to tune  $\alpha$  and  $\beta$  to get close to the analytical solution of Ref. [88] in dimension  $d = 0$  or our simulation results in dimension  $d = 1$ . Moreover, whenever we achieved a monotonic decay around  $w = 0$ , the result for  $\Delta(w)$  achieved by this transformation did not seem to depend on the dimension  $d$ , and the resulting curves lay way beyond the 1-loop curve, as can be seen on Fig. 17.

#### APPENDIX G: INDEPENDENCE OF $\mathcal{B}$ ON THE ELASTIC COEFFICIENT $c$

To demonstrate that the universal amplitude  $\mathcal{B}$  defined in Eq. (108) is independent of the elastic coefficient  $c$ , we perform simulations for different values of  $c$ . The results are presented in Table III and Fig. 18. Within error bars,  $\mathcal{B}$  does not change with  $c$ . Figure 18 shows the dependence of the rescaled correlation length  $\hat{\rho} := \rho_m m^\zeta$  on  $c$ . We observe an increase of  $\hat{\rho}$  for  $c < 1$ , which can be explained as follows. Making  $c$  and  $m$  smaller (we fix  $mL = 4\sqrt{c}$ ) renders the interface fluctuations larger, allowing it to explore more disorder configurations. As a consequence,  $\hat{\rho}$  slightly increases. This shows numerically that, while  $\mathcal{B}$  is universal,  $\hat{\rho}$  is not.

- [1] B. Alessandro, C. Beatrice, G. Bertotti, and A. Montorsi, Domain-wall dynamics and Barkhausen effect in metallic ferromagnetic materials. I. Theory, *J. Appl. Phys.* **68**, 2901 (1990).
- [2] G. Durin and S. Zapperi, Scaling exponents for Barkhausen avalanches in polycrystalline and amorphous ferromagnets, *Phys. Rev. Lett.* **84**, 4705 (2000).
- [3] M. Huth, P. Haibach, and H. Adrian, Scaling properties of magnetic domain walls in Pt/Co/Pt trilayers

on MgO (111), *J. Magn. Magn. Mater.* **240**, 311 (2002).

- [4] B. Cerruti, G. Durin, and S. Zapperi, Hysteresis and noise in ferromagnetic materials with parallel domain walls, *Phys. Rev. B* **79**, 134429 (2009).
- [5] V. Jeudy, A. Mougin, S. Bustingorry, W. Savero Torres, J. Gorchon, A. B. Kolton, A. Lemaître, and J.-P. Jamet, Universal pinning energy barrier for driven domain walls in thin ferromagnetic films, *Phys. Rev. Lett.* **117**, 057201 (2016).

- [6] G. Durin, F. Bohn, M. A. Correa, R. L. Sommer, P. Le Doussal, and K. J. Wiese, Quantitative scaling of magnetic avalanches, *Phys. Rev. Lett.* **117**, 087201 (2016).
- [7] V. Jeudy, R. Díaz Pardo, W. Savero Torres, S. Bustingorry, and A. B. Kolton, Pinning of domain walls in thin ferromagnetic films, *Phys. Rev. B* **98**, 054406 (2018).
- [8] C. ter Burg, F. Bohn, G. Durin, R. L. Sommer, and K. J. Wiese, Force correlations in disordered magnets, *Phys. Rev. Lett.* **129**, 107205 (2022).
- [9] B. Gutenberg and C. F. Richter, Frequency of earthquakes in California, *Bull. Seismological Soc. Am.* **34**, 185 (1944).
- [10] B. Gutenberg and C. F. Richter, Earthquake magnitude, intensity, energy, and acceleration, *Bull. Seismological Soc. Am.* **46**, 105 (1956).
- [11] Y. Ben-Zion and J. R. Rice, Earthquake failure sequences along a cellular fault zone in a three-dimensional elastic solid containing asperity and nonasperity regions, *J. Geophys. Res.* **98**, 14109 (1993).
- [12] J. M. Carlson, J. S. Langer, and B. E. Shaw, Dynamics of earthquake faults, *Rev. Mod. Phys.* **66**, 657 (1994).
- [13] D. Fisher, K. Dahmen, S. Ramanathan, and Y. Ben-Zion, Statistics of earthquakes in simple models of heterogeneous faults, *Phys. Rev. Lett.* **78**, 4885 (1997).
- [14] D. S. Fisher, Collective transport in random media: From superconductors to earthquakes, *Phys. Rep.* **301**, 113 (1998).
- [15] Y. Y. Kagan, Seismic moment distribution revisited: I. Statistical results, *Geophys. J. Int.* **148**, 520 (2002).
- [16] E. A. Jagla and A. B. Kolton, A mechanism for spatial and temporal earthquake clustering, *J. Geophys. Res.* **115**, B05312 (2009).
- [17] F. Brochard and P. G. De Gennes, Collective modes of a contact line, *Langmuir* **7**, 3216 (1991).
- [18] L. A. Amaral, A. L. Barabási, and H. E. Stanley, Universality classes for interface growth with quenched disorder, *Phys. Rev. Lett.* **73**, 62 (1994).
- [19] E. Rolley, C. Guthmann, R. Gombrowicz, and V. Repain, Roughness of the contact line on a disordered substrate, *Phys. Rev. Lett.* **80**, 2865 (1998).
- [20] A. Prevost, E. Rolley, and C. Guthmann, Dynamics of a helium-4 meniscus on a strongly disordered cesium substrate, *Phys. Rev. B* **65**, 064517 (2002).
- [21] S. Moulinet, A. Rosso, W. Krauth, and E. Rolley, Width distribution of contact lines on a disordered substrate, *Phys. Rev. E* **69**, 035103(R) (2004).
- [22] E. Rolley and C. Guthmann, Dynamics and hysteresis of the contact line between liquid hydrogen and cesium substrates, *Phys. Rev. Lett.* **98**, 166105 (2007).
- [23] A. Rosso and W. Krauth, Roughness at the depinning threshold for a long-range elastic string, *Phys. Rev. E* **65**, 025101(R) (2002).
- [24] C. Bachas, P. Le Doussal, and K. J. Wiese, Wetting and minimal surfaces, *Phys. Rev. E* **75**, 031601 (2007).
- [25] S. Scheidl and V. M. Vinokur, Driven dynamics of periodic elastic media in disorder, *Phys. Rev. E* **57**, 2574 (1998).
- [26] K. E. Bassler and M. Paczuski, Simple model of superconducting vortex avalanches, *Phys. Rev. Lett.* **81**, 3761 (1998).
- [27] P. Le Doussal, Z. Ristivojevic, and K. J. Wiese, Exact form of the exponential correlation function in the glassy super-rough phase, *Phys. Rev. B* **87**, 214201 (2013).
- [28] T. Emig and T. Nattermann, Effect of planar defects on the stability of the Bragg glass phase of type-II superconductors, *Phys. Rev. Lett.* **97**, 177002 (2006).
- [29] T. Giamarchi and P. Le Doussal, Elastic theory of flux lattices in the presence of weak disorder, *Phys. Rev. B* **52**, 1242 (1995).
- [30] K. J. Wiese and A. A. Fedorenko, Depinning transition of charge-density waves: Mapping onto  $O(n)$  symmetric  $\phi^4$  theory with  $n \rightarrow -2$  and loop-erased random walks, *Phys. Rev. Lett.* **123**, 197601 (2019).
- [31] T. Emig and T. Nattermann, A new disorder-driven roughening transition of charge-density waves and flux-line lattices, *Phys. Rev. Lett.* **79**, 5090 (1997).
- [32] L. W. Chen, L. Balents, M. P. A. Fisher, and M. C. Marchetti, Dynamical transition in sliding charge-density waves with quenched disorder, *Phys. Rev. B* **54**, 12798 (1996).
- [33] K. J. Wiese, Theory and experiments for disordered elastic manifolds, depinning, avalanches, and sandpiles, *Rep. Prog. Phys.* **85**, 086502 (2022).
- [34] K. Wilson and J. Kogut, The renormalization group and the  $\epsilon$ -expansion, *Phys. Rep.* **12**, 75 (1974).
- [35] F. J. Wegner and A. Houghton, Renormalization group equation for critical phenomena, *Phys. Rev. A* **8**, 401 (1973).
- [36] D. S. Fisher, Random fields, random anisotropies, nonlinear sigma models and dimensional reduction, *Phys. Rev. B* **31**, 7233 (1985).
- [37] D. S. Fisher, Sliding charge-density waves as a dynamical critical phenomena, *Phys. Rev. B* **31**, 1396 (1985).
- [38] D. S. Fisher, Interface fluctuations in disordered systems:  $5 - \epsilon$  expansion, *Phys. Rev. Lett.* **56**, 1964 (1986).
- [39] A. A. Middleton and D. S. Fisher, Critical behavior of pinned charge-density waves below the threshold for sliding, *Phys. Rev. Lett.* **66**, 92 (1991).
- [40] O. Narayan and D. S. Fisher, Critical behavior of sliding charge-density waves in  $4-\epsilon$  dimensions, *Phys. Rev. B* **46**, 11520 (1992).
- [41] O. Narayan and D. S. Fisher, Dynamics of sliding charge-density waves in  $4-\epsilon$  dimensions, *Phys. Rev. Lett.* **68**, 3615 (1992).
- [42] O. Narayan and D. S. Fisher, Threshold critical dynamics of driven interfaces in random media, *Phys. Rev. B* **48**, 7030 (1993).
- [43] L. Balents and D. S. Fisher, Large- $N$  expansion of  $(4-\epsilon)$ -dimensional oriented manifolds in random media, *Phys. Rev. B* **48**, 5949 (1993).
- [44] T. Nattermann, S. Stepanow, L.-H. Tang, and H. Leschhorn, Dynamics of interface depinning in a disordered medium, *J. Phys. II France* **2**, 1483 (1992).
- [45] H. Leschhorn, T. Nattermann, S. Stepanow, and L.-H. Tang, Driven interface depinning in a disordered medium, *Ann. Phys. (Leipzig)* **509**, 1 (1997).
- [46] P. Chauve, P. Le Doussal, and K. J. Wiese, Renormalization of pinned elastic systems: How does it work beyond one loop? *Phys. Rev. Lett.* **86**, 1785 (2001).
- [47] P. Le Doussal, K. J. Wiese, and P. Chauve, 2-loop functional renormalization group analysis of the depinning transition, *Phys. Rev. B* **66**, 174201 (2002).
- [48] P. Le Doussal, K. J. Wiese, and P. Chauve, Functional renormalization group and the field theory of disordered elastic systems, *Phys. Rev. E* **69**, 066107 (2004).

- [49] P. Le Doussal and K. J. Wiese, Size distributions of shocks and static avalanches from the functional renormalization group, *Phys. Rev. E* **79**, 051106 (2009).
- [50] P. Le Doussal, A. A. Middleton, and K. J. Wiese, Statistics of static avalanches in a random pinning landscape, *Phys. Rev. E* **79**, 050101(R) (2009).
- [51] A. Rosso, P. Le Doussal, and K. J. Wiese, Avalanche-size distribution at the depinning transition: A numerical test of the theory, *Phys. Rev. B* **80**, 144204 (2009).
- [52] P. Le Doussal and K. J. Wiese, First-principle derivation of static avalanche-size distribution, *Phys. Rev. E* **85**, 061102 (2012).
- [53] P. Le Doussal and K. J. Wiese, *Dynamics of Avalanches* (unpublished).
- [54] A. Dobrinevski, P. Le Doussal, and K. J. Wiese, Non-stationary dynamics of the Alessandro-Beatrice-Bertotti-Montorsi model, *Phys. Rev. E* **85**, 031105 (2012).
- [55] P. Le Doussal and K. J. Wiese, Distribution of velocities in an avalanche, *Europhys. Lett.* **97**, 46004 (2012).
- [56] P. Le Doussal, A. Petković, and K. J. Wiese, Distribution of velocities and acceleration for a particle in Brownian correlated disorder: Inertial case, *Phys. Rev. E* **85**, 061116 (2012).
- [57] A. Dobrinevski, P. Le Doussal, and K. J. Wiese, Statistics of avalanches with relaxation and Barkhausen noise: A solvable model, *Phys. Rev. E* **88**, 032106 (2013).
- [58] P. Le Doussal and K. J. Wiese, Avalanche dynamics of elastic interfaces, *Phys. Rev. E* **88**, 022106 (2013).
- [59] A. Dobrinevski, P. Le Doussal, and K. J. Wiese, Avalanche shape and exponents beyond mean-field theory, *Europhys. Lett.* **108**, 66002 (2014).
- [60] Z. Zhu and K. J. Wiese, The spatial shape of avalanches, *Phys. Rev. E* **96**, 062116 (2017).
- [61] A. A. Middleton, P. Le Doussal, and K. J. Wiese, Measuring functional renormalization group fixed-point functions for pinned manifolds, *Phys. Rev. Lett.* **98**, 155701 (2007).
- [62] A. Rosso, P. Le Doussal, and K. J. Wiese, Numerical calculation of the functional renormalization group fixed-point functions at the depinning transition, *Phys. Rev. B* **75**, 220201(R) (2007).
- [63] P. Le Doussal, K. J. Wiese, S. Moulinet, and E. Rolley, Height fluctuations of a contact line: A direct measurement of the renormalized disorder correlator, *Europhys. Lett.* **87**, 56001 (2009).
- [64] K. J. Wiese, M. Bercy, L. Melkonyan, and T. Bizebard, Universal force correlations in an RNA-DNA unzipping experiment, *Phys. Rev. Res.* **2**, 043385 (2020).
- [65] C. ter Burg, P. Rissone, M. Rico-Pasto, F. Ritort, and K. J. Wiese, Experimental test of Sinai's model in DNA unzipping, *Phys. Rev. Lett.* **130**, 208401 (2023).
- [66] K. J. Wiese, C. Husemann, and P. Le Doussal, Field theory of disordered elastic interfaces at 3-loop order: The  $\beta$ -function, *Nucl. Phys. B* **932**, 540 (2018).
- [67] C. Husemann and K. J. Wiese, Field theory of disordered elastic interfaces to 3-loop order: Results, *Nucl. Phys. B* **932**, 589 (2018).
- [68] This happens, e.g., in DNA peeling or unzipping experiments, where fluctuations of the bead diameter used in the optical trap induce fluctuations in  $m^2$ .
- [69] J. Cardy, Logarithmic conformal field theories as limits of ordinary CFTs and some physical applications, *J. Phys. A* **46**, 494001 (2013).
- [70] J. Cardy, Logarithmic correlations in quenched random magnets and polymers, [arXiv:cond-mat/9911024](https://arxiv.org/abs/cond-mat/9911024).
- [71] P. C. Martin, E. D. Siggia, and H. A. Rose, Statistical dynamics of classical systems, *Phys. Rev. A* **8**, 423 (1973).
- [72] H.-K. Janssen, On a Lagrangean for classical field dynamics and renormalization group calculations of dynamical critical properties, *Z. Phys. B* **23**, 377 (1976).
- [73] C. De Dominicis, Techniques de renormalisation de la théorie des champs et dynamique des phénomènes critiques, *J. Phys. Colloques* **37**, C1-247 (1976).
- [74] H. K. Janssen, *Feldtheoretische Methoden in der Statistischen Mechanik*, Vorlesungsmanuskript Uni Düsseldorf (1985).
- [75] U. Täuber, *Critical Dynamics: A Field Theory Approach to Equilibrium and Non-Equilibrium Scaling Behavior* (Cambridge University Press, Cambridge, 2012).
- [76] A. N. Vasilev, *The Field Theoretic Renormalization Group in Critical Behavior Theory and Stochastic Dynamics* (Chapman and Hall/CRC, New York, 2004).
- [77] A. A. Middleton, Asymptotic uniqueness of the sliding state for charge-density waves, *Phys. Rev. Lett.* **68**, 670 (1992).
- [78] Note that these relations are rather sensitive to muddling with coefficients: Multiplying any of the coefficients with a factor of  $b$  shows that the solution depends on  $b$  with a factor of at least  $0.1b$  and  $\max 1.3b$ . Thus, an error made in  $a_1$ ,  $a_2$ , and  $a_3$  has a strong impact on the final result.
- [79] The reader can verify that, when expanded in  $\epsilon$ , this equation gives back the original series.
- [80] A. Shapira and K. J. Wiese, Anchored advected interfaces, Oslo model, and roughness at depinning, *J. Stat. Mech.* (2023) 063202.
- [81] K. J. Wiese and A. A. Fedorenko, Field theories for loop-erased random walks, *Nucl. Phys. B* **946**, 114696 (2019).
- [82] T. Helmuth and A. Shapira, Loop-erased random walk as a spin system observable, *J. Stat. Phys.* **181**, 1306 (2020).
- [83] A. Shapira and K. J. Wiese, An exact mapping between loop-erased random walks and an interacting field theory with two fermions and one boson, *SciPost Phys.* **9**, 063 (2020).
- [84] M. Kompaniets and K. J. Wiese, Fractal dimension of critical curves in the  $O(n)$ -symmetric  $\phi^4$ -model and crossover exponent at 6-loop order: Loop-erased random walks, self-avoiding walks, Ising, XY and Heisenberg models, *Phys. Rev. E* **101**, 012104 (2020).
- [85] M. V. Kompaniets and E. Panzer, Minimally subtracted six-loop renormalization of  $O(n)$ -symmetric  $\phi^4$  theory and critical exponents, *Phys. Rev. D* **96**, 036016 (2017).
- [86] J. Bezanson, A. Edelman, S. Karpinski, and V. B. Shah, Julia: A fresh approach to numerical computing, *SIAM Rev.* **59**, 65 (2017).
- [87] A. Rosso and W. Krauth, Origin of the roughness exponent in elastic strings at the depinning threshold, *Phys. Rev. Lett.* **87**, 187002 (2001).
- [88] P. Le Doussal and K. J. Wiese, Driven particle in a random landscape: disorder correlator, avalanche distribution and extreme value statistics of records, *Phys. Rev. E* **79**, 026701 (2009).
- [89] G. Mukerjee and K. J. Wiese, Depinning in the quenched Kardar-Parisi-Zhang class II: Field theory, *Phys. Rev. E* **107**, 054137 (2023).



- [90] M. Abramowitz and A. Stegun, *Pocketbook of Mathematical Functions* (Harri-Deutsch-Verlag, Frankfurt am Main, 1984).
- [91] C. ter Burg and K. J. Wiese, Mean-field theories for depinning and their experimental signatures, *Phys. Rev. E* **103**, 052114 (2021).
- [92] P.G. de Gennes, Exponents for the excluded volume problem as derived by the Wilson method, *Phys. Lett. A* **38**, 339 (1972).
- [93] Contrary to the conventions Cardy uses in Ref. [70], we divided  $\mathcal{E}$  by  $n$  to simplify notations. These are the conventions he later used in Ref. [69].